Spring 2022

Design and Application of Membrane Nanodiscs for Biophysical Studies of Influenza A Proteins

Aye K. Kyaw , '22

Design and Application of Membrane Nanodiscs for Biophysical Studies of Influenza A Proteins

Presented as a Senior Course Thesis in Chemistry

Aye Kyaw

Department of Chemistry and Biochemistry

Swarthmore College

May 13th, 2022

Advisor: Dr. Kathleen P. Howard

Table of Contents

List of Figures and Tables

List of Common Abbreviations

AEBSF – 4-(2-aminoethyl) benzene sulfonyl fluoride hydrochloride

AH – amphipathic helix

CW – continuous wave

DLS – dynamic light scattering

DTT – dithiothreitol

EDTA – ethylenediamine-N,N,N',N'-tetraacetic acid

EPR – electron paramagnetic resonance

FPLC – fast protein lipid chromatography

GuHCl – guanidinium chloride

IAV – influenza A virus

M1 – matrix protein 1 from influenza A virus

M2 – matrix protein 2 from influenza A virus

MTSL – S-(1-oxyl-2,2,5,5-tetramethyl-2,5-dihydro- 1H-pyrrol-3-yl) methyl methanesulfonothioate spin-label

MP – membrane protein

MSP – membrane scaffold protein

OG – octyl β-D-glucopyranoside

PDB – protein data bank

POPC – 1-palmitoyl-2-oleoyl-*sn*-glycero-3-phosphocholine

POPG – 1-palmitoyl-2-oleoyl -*sn*-glycero-3[phosphor-*rac*-(1glycerol)]

RNP – ribonucleoprotein

SDS-PAGE – sodium dodecyl sulfate-polyacrylamide gel electrophoresis

SDSL – site-directed spin-labeling

SEC – size exclusion chromatography

TM – transmembrane

WT – wild-type

Abstract

Membrane proteins play a range of important roles in biological systems, yet they are underrepresented in the data base of high-resolution structures of all proteins. There is intense interest in developing new methodologies for studying membrane proteins. An essential step to membrane protein method development is devising reliable membrane mimics in which to embed membrane proteins.

The goal of this thesis was to develop and apply nanodisc membrane mimics to the study of an influenza A membrane protein called M2. Nanodiscs provide a lipid bilayer environment with access to both sides of the bilayer and are smaller than commonly used liposome model membranes whose size provides challenges for some biophysical methods. This thesis shows how the sample composition of M2 containing nanodiscs was optimized. Dynamic light scattering and size exclusion chromatography was used to characterize M2-nanodiscs.

Electrophysiological and budding assays showed that M2 in liposomes were in a functionally relevant conformation. Extensive previous work has been done on studying M2 protein in spherical liposome using site-directed spin label electron paramagnetic resonance (SDSL-EPR). We carried out SDSL-EPR studies of M2-nanodiscs and compared them to published work on M2 in liposomes. Our EPR data is consistent with M2 protein in nanodiscs having a similar conformation, mobility and membrane topology as that seen in previously published M2-liposome work. Furthermore, we probed the ability of nanodiscs to allow for conformational exchange by comparing the impact of drug binding on M2-nanodiscs with M2-liposomes.

Chapter 1: Introduction

1.1. Importance of Model Membranes for Understanding Membrane Proteins

Membrane proteins (MPs) play an important role in numerous biological processes, such as signal transduction, proton channels, and metabolic pathways. MPs represent between 20 and 30% of the human genome, and many serve as drug targets.[1–3] Due to their importance in the advancement of developing therapeutic drugs, it is essential to have a detailed structural understanding of the MPs. An intense area of interest is viral MPs. Viral MPs can facilitate viral entry into host cells, activate the viral uncoating, and play a key role in the budding of newly formed viruses.

Despite their importance, only about 3% of 100,000 protein structures available in the Protein Data Bank (PDB) are labeled as the MPs.[2] There are many reasons why the MPs are very challenging to study from a structural perspective. They are difficult to overexpress, purify, and require a hydrophobic environment to retain their native conformation and functionality. Although biological membranes extracted from cells can be used in biophysical studies of MPs, the heterogeneity of the complex mixtures poses great challenges for making reproducible samples. Therefore, a number of model membrane systems have been developed to make tractable systems appropriate for detailed biophysical work. Depending on the biophysical method employed and the questions to be answered, investigators use different model membranes.

Different membrane mimetics can impact the MP's conformation and functional activities.[4,5] For example, varying the types or compositions of lipids, bilayer thickness, or the lateral pressure of the liposomes altered the conformation of the MP under

investigation (Fig 1.1).[5,6] A detailed understanding membrane mimetics is essential in selecting a membrane system to be used for structure determination.

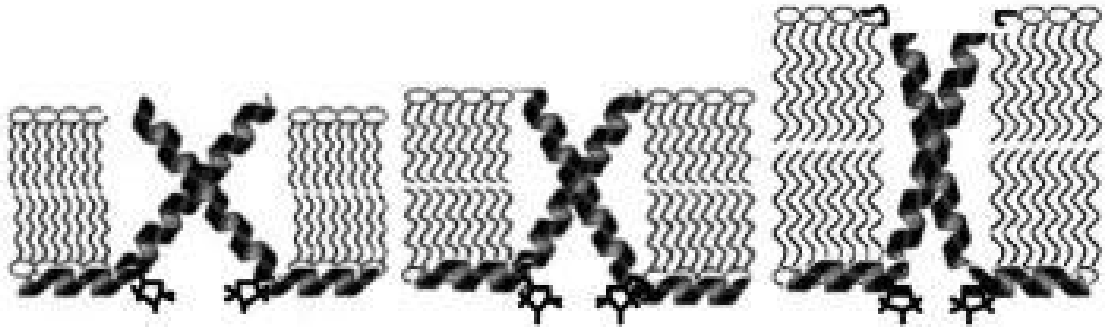

Figure 1.1. Conformational change in the membrane proteins due to a change in bilayer thickness. Membrane proteins are represented by α-helix dimer. Phospholipid bilayers are represented by the oval-head with a wriggly tail. Adapted from Saotome et al., 2015.5

Commonly used membrane mimetics include micelles, bicelles, liposomes, and nanodiscs (Fig. 1.2). Micelles are formed by self-assembly of amphiphilic molecules (detergents and surfactants) usually spherical, ranging in size from 2 to 20 nm depending on the concentration. Even though mild detergent micelles can solubilize the MPs in their native structure, the curvature and surface properties of micelles are significantly different from physiologically relevant cell membranes.[2] Bicelles contain a lipid bilayer surrounded by the detergent, but the morphology and stability of the resulting disc shaped mimics can vary with sample composition.

Nanodiscs and liposomes are currently two of the most popular model membranes used for biophysical studies. Nanodiscs are discs of lipid bilayer surrounded by a scaffold protein. Nanodisc's size can range from 8 to 16 nm, depending on the length of the scaffold protein used. Liposomes are sealed spherical lipid bilayers formed from hydrated phospholipids. Different sized liposomes have different degrees of membrane curvature. Each membrane system is composed differently so care should be taken to select the most

appropriate one for the MPs of interest. The optimal composition of the chosen membrane model depends on the size and shape of each MPs. The goal of this thesis is to optimize the composition of nanodiscs for the study of one of the influenza A membrane proteins.

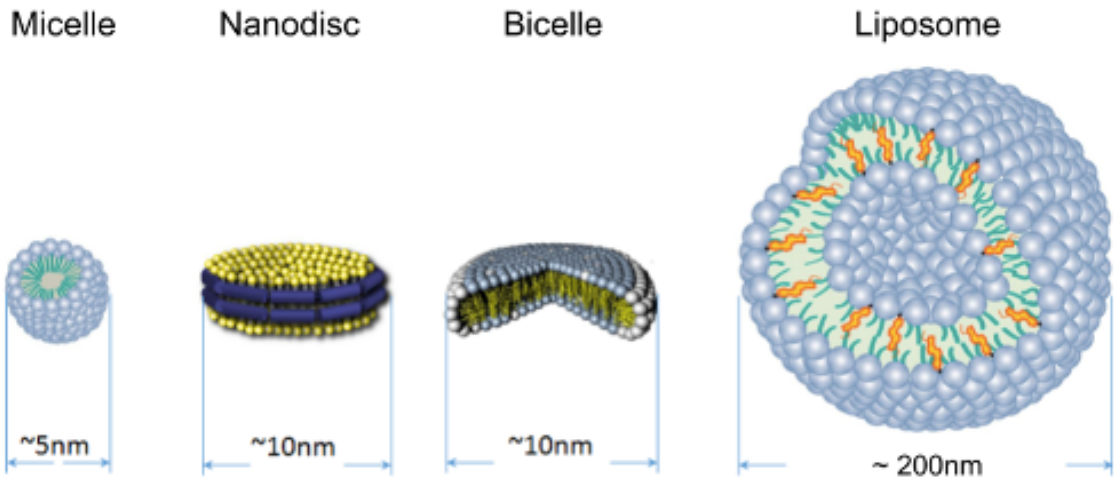

Figure 1.2. Comparison of model membrane mimics (not to scale). Approximate diameters are included at the bottom. Phospholipids are represented by the balls with wriggly colored lines. Membrane scaffold proteins are shown in dark blue long rods in nanodisc.

1.2. Nanodiscs Membrane Model

Nanodiscs are discoidal lipid bilayer membranes stabilized and solubilized in aqueous solution by two encircling amphipathic α-helical proteins, termed membrane scaffold proteins (MSPs). MSPs are genetically engineered from the sequence of human serum apolipoprotein A-1, and they can self-assemble into a cylindrical shaped disc in the presence of phospholipids (Fig. 1.3).[8,9] Human serum apolipoprotein A-1 transports excess cholesterol from peripheral cells to the liver. The empty nanodiscs were first generated in 2002,[8] and since then, they have been widely used in structural characterizations of multiple MPs with MSPs of varying lengths and in different bilayer environments.[4,7,10–14] In many cases nanodiscs are more stable compared to liposomes.[7]

Therefore, the nanodisc model has recently gained more attention as a valuable tool for biophysical functional studies of the MPs.

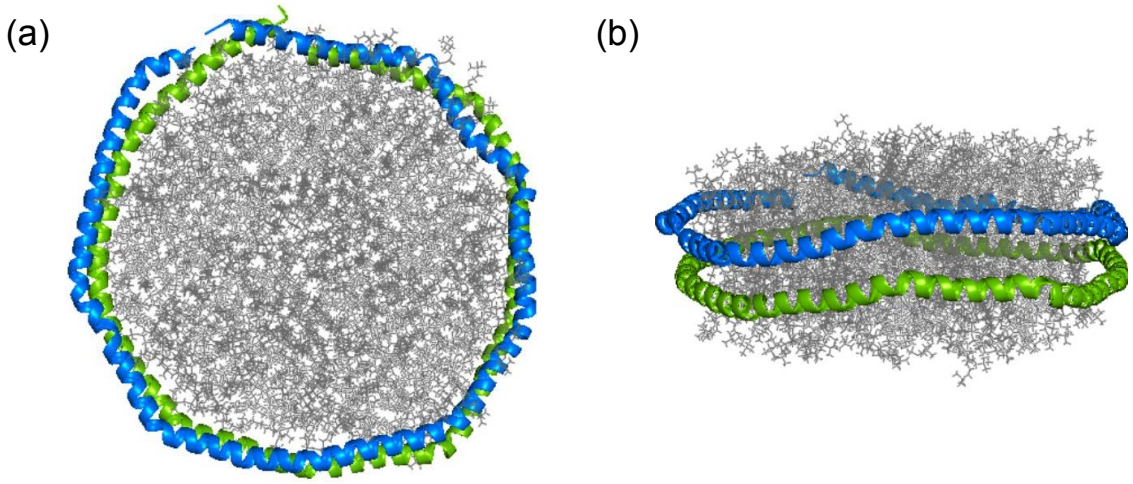

Figure 1.3. Cartoon of nanodisc. Nanodisc is composed of phospholipids and membrane scaffold proteins shown in (a) top view, and (b) side view. Two identical MSPs are represented by blue and green helices. Phospholipids are represented by the gray patch inside circular MSPs. Adapted from PDB: 2clz.[15]

1.3. Membrane Protein: The Matrix Protein 2

The matrix protein 2 (M2) of the Influenza A viruses (IAVs) is the MPs of interest in this study. M2 plays an important role in viral uncoating during infection as well as viral assembly during budding. M2 is a 97 amino acid integral membrane protein, encoded by nucleotides 26 to 51 and 740 to 1004 of M gene.[16] M2 can be divided into three domains: N-terminal ectodomain (residues 1 to 21), a transmembrane (TM) helix (residues 22 to 46) connected to an amphipathic helix (AH) (residues 47 to 62), and a C-terminal cytoplasmic tail (residues 63 to 97) (Fig. 1.4a).[17–20] M2 forms a homotetramer, allowing it to act as a proton channel. The transmembrane helix domain, which makes up this proton channel, has been extensively studied because of its important role in viral uncoating. The structure of the proton channel has been reported using multiple techniques, such as solid state NMR,[21] solution NMR,[22] X-ray crystallography,[23–25] and

electron paramagnetic resonance (EPR)[26] (Fig. 1.4b). The inconsistencies in the published structures of M2 were suspected to be due to different compositions of membrane environments, length of MPs, and sample preparation methods.[5] Figure 1.4b shows that X-ray crystallography uses only the transmembrane region of M2 (green and dark blue), and solid state NMR and solution NMR use the truncated M2 (red and light blue), and EPR uses the full length M2 (yellow). In addition, each group uses different membrane mimetics.

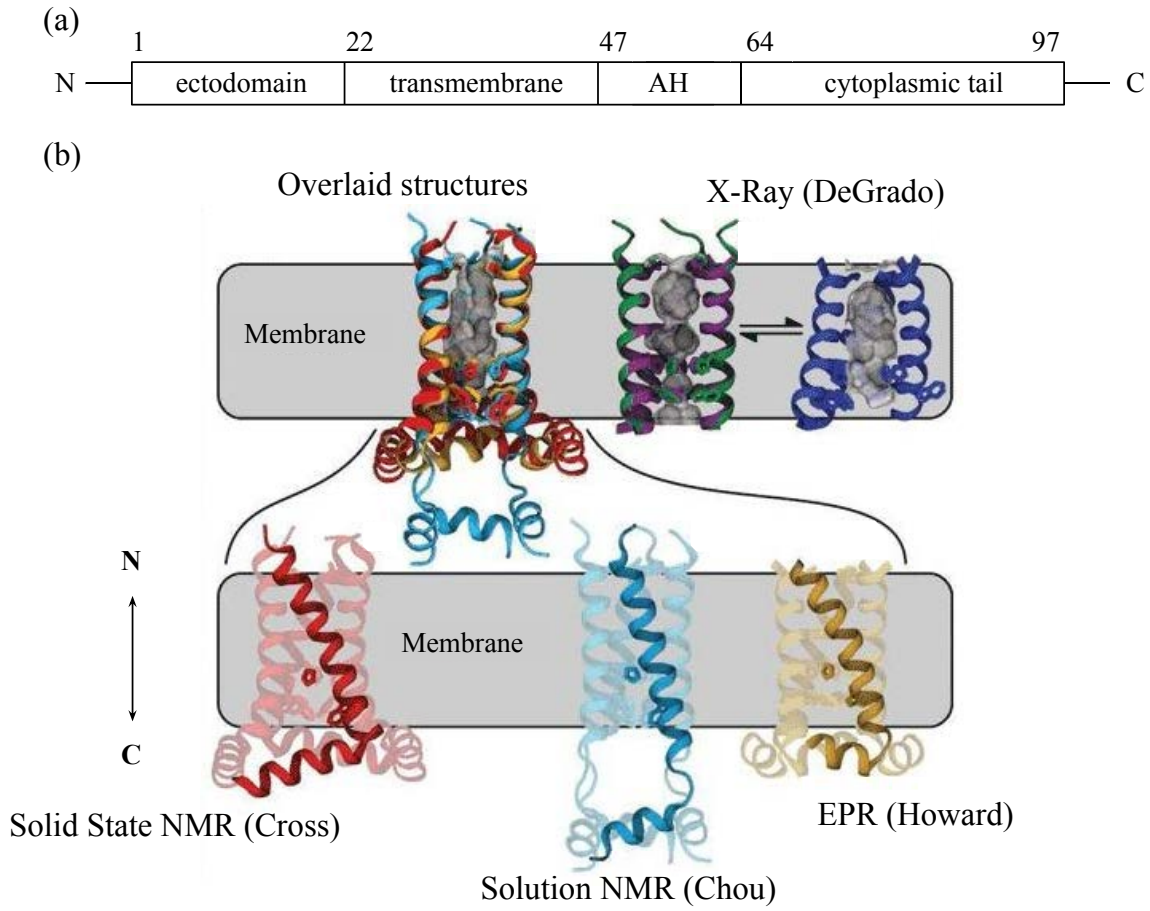

Figure 1.4. Comparison of M2 structures. (a) Domain map of M2 showing ectodomain, transmembrane region, amphipathic helix (AH), and C-terminal domain. (b) Previously published structures of M2 solved by different techniques. Structure solved by solid state NMR (red and purple),[21] solution NMR (light blue),[22] X-ray crystallography (green and dark blue)[23–25] and EPR (yellow).[26] Overlay of bottom structures (labeled Overlaid structures) shows differences in cytoplasmic tail of M2. AH: amphipathic helix. Adapted from Fiorin et al., 2010.[27]

Previous reports from the Howard lab have studied the multiple conformational substates of M2 in different pH[26] and membrane environments.[5,6,28] EPR data has been collected on 29 different spin labeled sites on M2 protein incorporated into lipid bilayers, The majority of the data has been collected in 4:1 1-palmitoyl-2-oleoyl-*sn* -glycero-3-phosphocholine:1-palmitoyl-2-oleoyl -*sn*-glycero-3[phosphor-*rac*-(1glycerol)] (POPC:POPG) liposome bilayer environment, and this is the lipid composition used in this thesis.[29-31]

Conformational exchange is an essential property of the M2 protein. For example, M2 monomers within the tetramer rearrange with pH which is important to viral uncoating at low pH.[26] The conformational state of M2 in cholesterol rich budozone differs from non-cholesterol containing.[6] There are conformational changes in M2 induced by antiviral drugs.[28] Thus, another goal of this thesis is to determine if conformational changes previously seen in liposomes can be observed in nanodiscs.

1.4. Inspirations for the Incorporation of M2 in Nanodiscs

Studies have shown that M2 plays an important role in viral assembly and budding in addition to serving as a proton channel.[5] M2 works synergistically with the matrix protein 1 (M1) as well as other membrane proteins to recruit the viral genome to the viral budding site as well as to form the curvature necessary for the scission and viral release. Earlier studies on the interaction between M2 and M1 proteins in liposomes, were complicated due to the bilateral incorporation of M2 into liposomes. M2 can be incorporated into liposomes in two possible orientations: the C-terminal domain of M2 inside the liposomes or outside the liposomes (Fig. 1.4). The M1 binds to the C-terminal domain of M2 which is inaccessible when the C-terminal domain is enclosed within the

bilayer interior of the liposome. That initiates the search for a membrane mimic like nanodiscs that allow full access to both surfaces of the membrane. Nanodiscs are smaller in size than liposomes which is very useful for carrying out some of the EPR methods that are sensitive to tumbling rate and that provide valuable information on distances.[7]

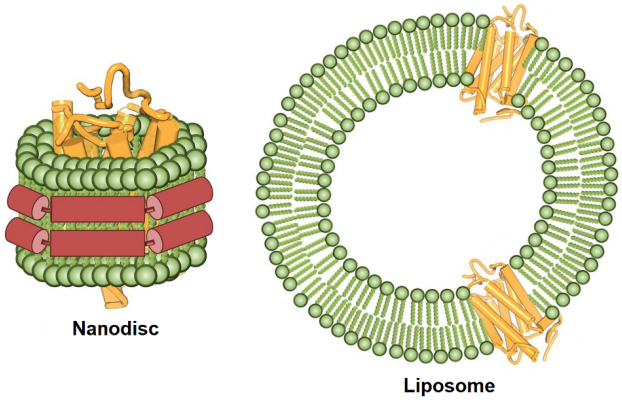

Figure 1.5. Incorporation of MP into nanodisc and liposome. Schematic of nanodisc showing membrane scaffold proteins (red) and unilateral incorporation of MP (yellow) on the left. Schematic of bilateral incorporation of MPs (yellow) into proteoliposome on the right. Phospholipids are shown in green balls and sticks.

1.5. Techniques for Studying Conformation and Dynamics of Membrane Proteins in Nanodiscs

This thesis presents how the M2-nanodiscs system was optimized. Dynamic Light Scattering (DLS) and Fast Protein Lipid Chromatography – Size Exclusion Chromatography (FPLC-SEC) were used to characterize the physical properties of the nanodiscs. SDSL-EPR technique is commonly used to characterize the conformation and dynamics of spin-labeled M2 incorporated in nanodisc membrane mimetics.[6,32] Structural parameters such as spin mobility and membrane accessibility with respect to membrane topology can be measured using SDSL-EPR (See Chapter 2, section 2.6.1 for details).

Chapter 2: Materials and Methods

2.1. Purification and Spin labeling of M2

The optimization and characterization of M2-nanodiscs required the overexpression and purification of full-length M2. A description of the plasmid and expression were previously published.[30,33] The sequences of the constructs expressed for this thesis are pasted below (Fig. 2.1).

```
M2 WT    MSLLTEVETPIRNEFGSRSNDSSDPLVVAASIIGILHLILWILDRLFFKSIYRFFEHGLK 60
M2 43C   MSLLTEVETPIRNEFGSRSNDSSDPLVVAASIIGILHLILWICDRLFFKSIYRFFEHGLK 60
M2 57C   MSLLTEVETPIRNEFGSRSNDSSDPLVVAASIIGILHLILWILDRLFFKSIYRFFECGLK 60
M2 68C   MSLLTEVETPIRNEFGSRSNDSSDPLVVAASIIGILHLILWILDRLFFKSIYRFFEHGLK 60
M2 82C   MSLLTEVETPIRNEFGSRSNDSSDPLVVAASIIGILHLILWILDRLFFKSIYRFFEHGLK 60

M2 WT    RGPSTEGVPESMREEYRKEQQSAVDADDSHFVSIELE          97
M2 43C   RGPSTEGVPESMREEYRKEQQSAVDADDSHFVSIELE          97
M2 57C   RGPSTEGVPESMREEYRKEQQSAVDADDSHFVSIELE          97
M2 68C   RGPSTEGCPESMREEYRKEQQSAVDADDSHFVSIELE          97
M2 82C   RGPSTEGVPESMREEYRKEQQCAVDADDSHFVSIELE          97
```

Figure 2.1. The sequence of M2 protein constructs. Sequence of full length M2 WT Udorn strain (A/Udorn/307/1972 (H3N2)) contains four extra mutations (highlighted in yellow) designed to enhance expression. The sites highlighted in green were mutated to cysteine so the spin label could be attached. M2 protein had a C-terminal His tag (not shown in sequences above) to facilitate purification.

The M2 purification and spin-labeling strategy for proteins used in this thesis shown in Scheme 2.1. The protocol is routinely optimized as equipment/materials are replaced. The spin-labeling step is skipped if unlabeled M2 is needed.

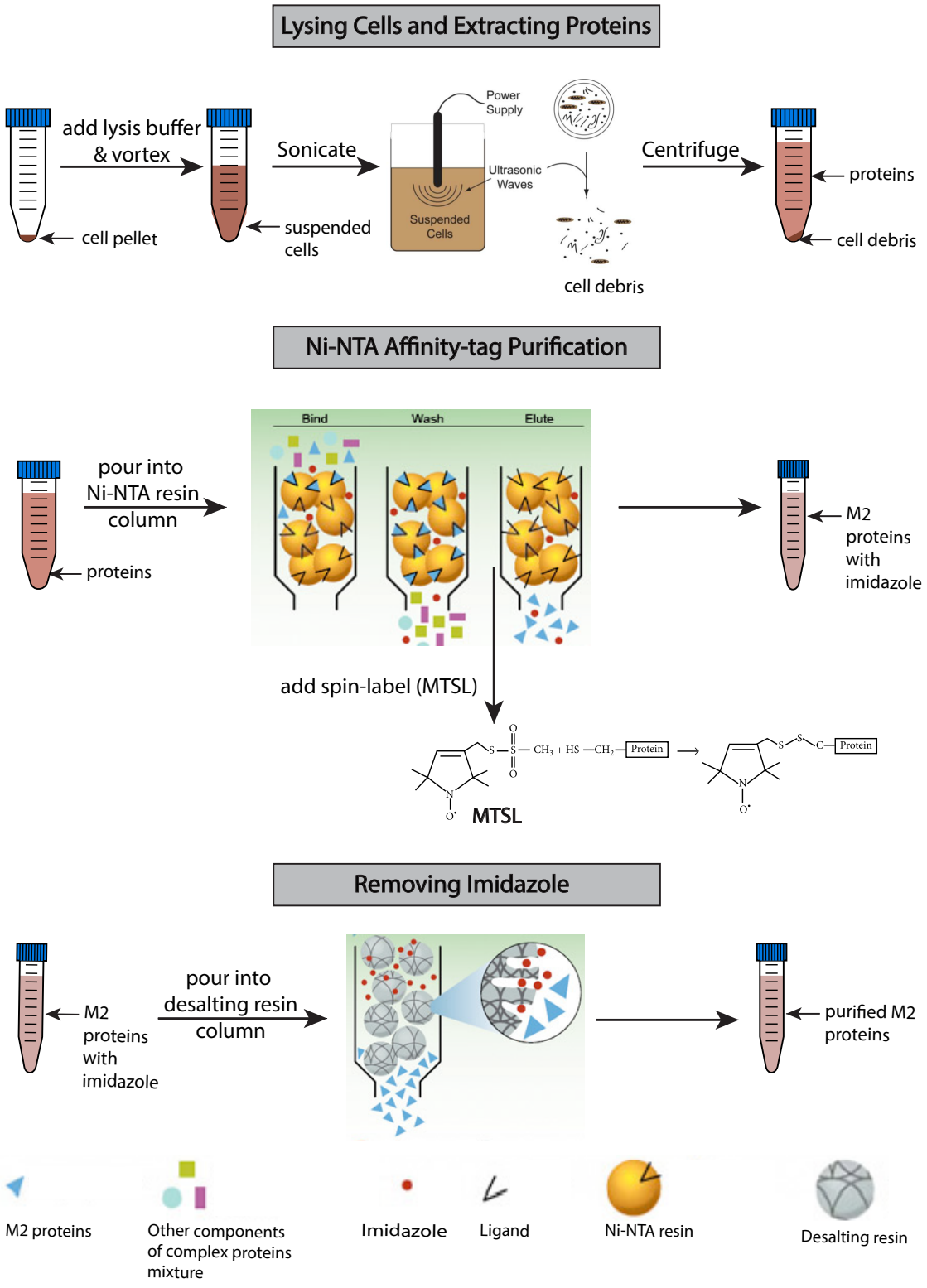

Scheme 2.1. Purification Scheme for full length M2. Removing imidazole step also removes free spin for spin-labeled M2 purification.

Purifications were done on different scales depending on intended application, but the majority of time, 250 mL of expressed cell pellet produces enough protein for a set of experiments. The yield of M2 purified protein per liter varies widely depending on the construct, but the typical range is 1-2 mg/mL for a 250 mL pellet. The purified protein degrades over time, so we only purify enough that can be used within 1-2 weeks. Protocol below is for 250 mL pellet.

For each M2 construct, overexpressed cell pellets from 250 mL of growth (A/Udorn/307/1972 (H3N2)) were incubated on ice in the Lysis Buffer (50 mM Tris pH 8, 150 mM NaCl, 20 mM imidazole, 30 mM octyl β-D-glucopyranoside (OG), 0.2 µg/mL DNase I, 500 µM 4-(2-aminoethyl) benzene sulfonyl fluoride hydrochloride (AEBSF), 0.25 µg/mL lysozyme) for about 30 min and vortexed to get a homogeneous cell solution. To obtain the protein expressed in the cells, they need to be broken open using the tip sonicator. The ¼″ probe tip sonicator instrument (Fisher Scientific) parameters (20 min on 20% amplitude, 1 second on/1 second off pulse) were applied to the suspended cell mixture on ice to break open the cell membrane. The cell mixture was then centrifuged at 16,000 rpm using Fiberlite F20-12x50 LEX Fixed Angle Rotor in a Sorvall LYNX 4000 Superspeed Centrifuge at 4°C for 30 min with 9 accel/5 decel to separate the solubilized proteins from the cell debris. After centrifugation, the post-lysis supernatant was separated from the pellet (which is cell debris, Scheme 2.1) and 5.0 µL β-mercapto-ethanol and 100 µL imidazole were added to the supernatant. This is to prevent nonspecific binding to the Ni-column of proteins that we don't want and to reduce disulfide bonding in proteins, which can lead to aggregation and precipitation. The supplemented post-lysis supernatant was then poured into a Ni-NTA column prepped

with 0.5 mL of HisPur™ Ni-NTA resin (ThermoScientific), saturated with 5 mL of 20 mM imidazole. Then the column was nutated at room temperature for 30 min to allow the His-tagged M2 to completely bind to the Ni-resin and let the supernatant flow through the Ni column. The Ni column was then washed subsequently with 5 mL each of Wash 1, Wash 2, Wash 3 in that order (Wash 1: 50 mM Tris pH 8, 150 mM NaCl, 30 mM OG, 20% v/v glycerol, Wash 2: 50 mM Tris pH 8, 30 mM OG, 20% v/v glycerol, Wash 3: 50 mM Tris pH 8, 30 mM OG, 20% v/v glycerol, 20 mM imidazole) to remove all the proteins except the His-tagged M2.

We spin label the proteins while the protein is still stuck to the column resin. For spin-labeling, 16 μL of 118 mM S-(1-oxyl-2,2,5,5-tetramethyl-2,5-dihydro-1H-pyrrol-3 -yl) methyl methanesulfonothioate (MTSL) in 1 mL of wash 3 was added to the Ni-column and nutated for 24-48 hours for complete spin-labeling reaction (Scheme 2.1). After 24-48 hours, the Ni-column was washed with 5 mL of Wash 2, and the protein was eluted off the column with Elution Buffer (50 mM Tris pH 8, 30 mM OG, 300 mM imidazole, 20% v/v glycerol), which has high amount of imidazole.

For M2 WT protein purification, the spin-labeling step was skipped, and the protein was eluted from the Ni-column right after Wash 3 with Elution Buffer. The eluted protein was buffer-swapped into Desalting Buffer (50 mM Tris pH 8, 30 mM OG) via PD-10 Desalting Column (GE Healthcare Life Sciences), to remove imidazole and/or excess spin-label in solution.

For the spin-labeled M2, the EPR spectrum of post-PD-10 M2 was necessary to verify the signal and check for free excess spin-label (Fig. 2.2). If the spectrum of the post-PD-10 M2 showed evidence of free spin (which presents a sharp triplet

superimposed on the much broader spectrum shown in Fig. 2.2), a second run through the PD-10 column was performed. The purity of pooled post-PD-10 M2 protein was verified via sodium dodecyl sulfate-polyacrylamide gel electrophoresis (SDS-PAGE) (Fig. 2.3). M2 appears as a monomer band (<15 kDa), although due to its strong homo-oligomeric hydrophobic association a fainter band that corresponds to a M2 dimer is often observed.

Figure 2.2. Represer **in check.** EPR spectrur ows no free excess s

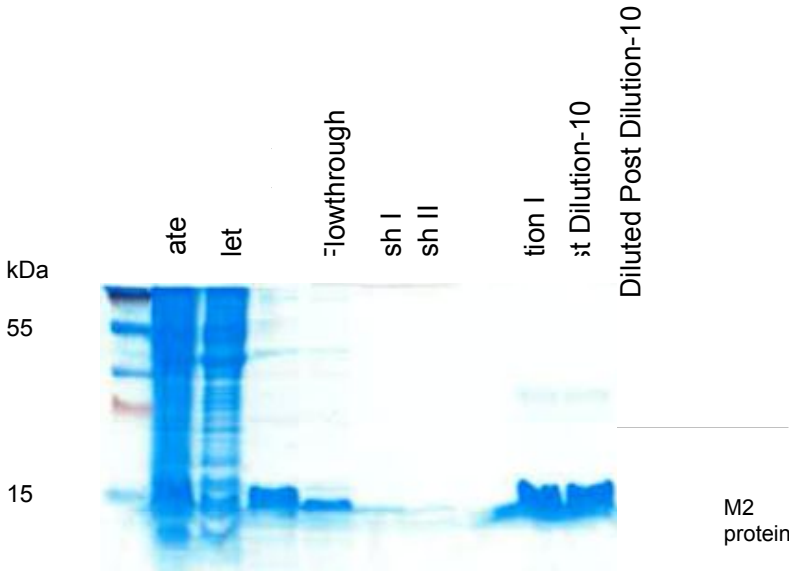

Figure 2.3. Representative gel for full length M2 purification. SDS-PAGE tracks M2 throughout successful purification of site 43 labeled full length M2. Monomeric M2 appears as a band at less than 15 kDa, corresponding to MW of 11.8 kDa.

2.2. Purification of Membrane Scaffold Proteins (MSP)

The MSP1D1 plasmid received as a gift from the Sanders Lab at Vanderbilt University was overexpressed in BL21 cells under kanamycin antibiotic control. The MSP1D1 construct contains a His-tag and a TEV cleavage site. MSP1D1 was expressed and purified based on a previously established protocol with some minor modifications.[10]

Briefly, a thawed MSP1D1 cell pellet was resuspended in 4 mL of Lysis Buffer (Buffer A (50 mM Tris-HCl, pH 8.0, 500 mM NaCl), 1% Triton X-100, and 1 mM EDTA) per gram of cell pellet and vortexed to get homogeneous cell mixture. Tip sonicator instrument parameters (3 min on 40% amplitude, 3 second on/7 second off pulse) were applied to the suspended cell mixture on ice to break open the cell membrane. 5 mM of $MgCl_2$ and 1 μg/mL of DNase I was added to the lysed cell solution and stirred on ice for 30 min. The cell mixture was then centrifuged at 15,800 rpm using Fiberlite F20-12x50 LEX Fixed Angle Rotor in a Sorvall LYNX 4000 Superspeed Centrifuge at 4°C for 45 min with 9 accel/5 decel to separate the solubilized proteins from the cell debris. After centrifugation, the post-lysis supernatant was separated from the pellet (which is cell debris).

The post-lysis supernatant was prepared by adding 2 M imidazole with the volume of 1% of the supernatant volume and poured into the Ni-NTA column prepped with 0.5 mL of HisPur™ Ni-NTA resin (ThermoScientific), saturated with 5 mL of MSP Wash I (Buffer A, 1% Triton X-100). The column was nutated at room temperature for 30 min to allow the His-tagged MSP1D1 to completely bind to the Ni-resin and the supernatant then flowed through the Ni column after 30 min. The Ni column was then washed subsequently with 5 mL each of MSP Wash 1, MSP Wash 2, MSP Wash 3, MSP

Wash 4 in that order (MSP Wash 2: Buffer A, 50 mM cholate, MSP Wash 3: Buffer A, MSP Wash 4: Buffer A, 20 mM imidazole) to remove all the proteins except His-tagged MSP1D1 protein. The MSP1D1 was eluted off the column with MSP Elution Buffer (Buffer A, 500 mM imidazole), which has a high amount of imidazole.

As much as half of the MSP1D1 protein expressed ends up in inclusion bodies found in the insoluble fraction after cell lysis. To improve the overall yield, the post-lysis pellet was resuspended in 6 M guanidinium chloride (GuHCl) in Buffer A. The resuspended cell pellet solution was centrifuged similarly to the post-lysis supernatant. The p-supernatant (supernatant of resuspended cell solution) is then separated from the p-pellet (pellet of resuspended cell solution) and poured into the Ni-column prepped with 5 mL of 6 M GuHCl in Buffer A. The p-supernatant was prepared, and the Ni-column was washed and eluted in the similar manner as the post-lysis supernatant.

The eluted fractions from post-lysis supernatant and p-supernatant were then combined to proceed with the His-tag cleavage. The eluted fractions were buffer swapped into Dialysis 1 (50 mM Tris, pH 8, 20 mM NaCl). (1% of MSP1D1 concentration) mg/mL of TEV (BioLabs) and 100 mM dithiothreitol (DTT) was added to post-Dialysis 1 to cleave the His-tag off MSP1D1. The resulting post-Dialysis 1 solution was then buffer-swapped into Dialysis 2 (20 mM Tris, pH 7.5, 500 mM NaCl) to remove DTT because DTT can ruin the Ni-column.

The post-Dialysis 2 solution was poured into the Ni-column equilibrated with a mixture of Dialysis 2 and 20 mM imidazole. This step is called a reverse Ni-column because in this case the TEV protease should have cut the His-tag off the MSP1D1 and therefore, the MSP1D1 without His-tag should not stick to the column, but the His-

Tagged TEV should stick to the column. The column was nutated as described above and the flowthrough was collected. The flowthrough contains the MSP1D1 without His-tag. The column was then washed with a mixture of Dialysis 2 and increasing imidazole to wash off the His-tagged TEV bound to the Ni-column. The flowthrough was then buffer swapped into Dialysis 3 (20 mM Tris, pH 7.5, 100 mM NaCl, 0.5 mM EDTA) so that it will be ready for the nanodisc preparation. The purity of the MSP1D1 and the successful cleavage by TEV is shown in Figure 2.4.

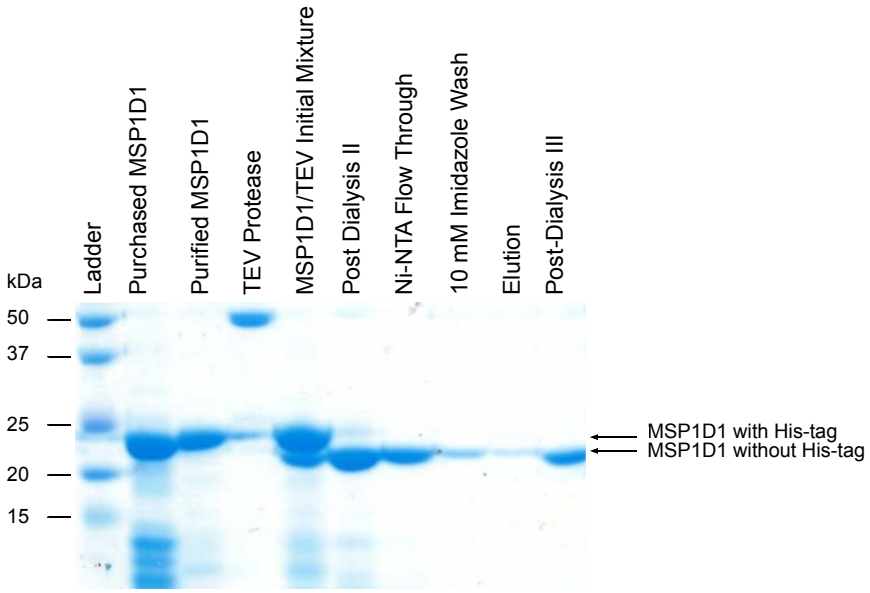

Figure 2.4. SDS-PAGE gel for MSP1D1 purification and His-tag removal. SDS-PAGE tracks MSP1D1 throughout successful purification of full length MSP1D1. His tag was removed using TEV protease. Early studies used MSP1D1 purchased from Cube Biotex and is shown in Lane 2.

2.3. Reconstitution of M2 into Proteoliposomes

Purified M2 was reconstituted into 4:1 POPC:POPG bilayers at a molar ratio of 1 to 500 (protein to lipid). Lipid films were solubilized in Extruder Buffer (50 mM Tris pH 7.8, 100 mM KCl, 1 mM EDTA) and extruded 15 times through a 200 nm filter using an Avanti Mini-Extruder to homogenize the liposome sizes. OG detergent was added to a concentration of 30 mM and the lipid-detergent mixture was equilibrated for 30 min. Purified M2 protein was added to the lipid-detergent solution such that M2 tetramer to lipid molar ratio is 1 to 200. Additional Extruder Buffer was added to dilute OG concentration to 15 mM, below the critical micelle concentration. A degassed slurry of hydrophobic polystyrene beads (Biobeads SM-2, Bio-Rad) in Extruder Buffer was added in aliquot of 50 µL over a period of an hour and incubated for additional 2 hours to facilitate the removal of detergent. Biobeads were removed and proteoliposomes were pelleted at 90,000 rpm in the TLA-100 rotor of an Optima-MAX-TL ultracentrifuge (Beckman-Coulter) for 1 hour at 4°C. All pellets were combined and resuspended in 200 µL of supernatant and re-pelleted under the same centrifugation settings and stored separately as pellet and supernatant at 4°C for further EPR studies.

2.4. Purification of Nanodiscs via Fast Protein Lipid Chromatography-Size Exclusion Chromatography (FPLC-SEC)

Fast protein liquid chromatography (FPLC) is a form of medium-pressure chromatography that uses a pump to control the speed at which the mobile phase passes through the stationary phase. Size exclusion chromatography (SEC), also known as gel filtration, separates molecules according to the differences in size as they pass through a

gel filtration medium packed in a column. The medium is a porous matrix of spherical particles. When the column is run, the bigger particles elute before the smaller particles.

For the optimization of nanodisc preparation with M2 WT protein, the nanodisc solution, prepared according to Scheme 3.1, was characterized using the Superdex 200 increase 10/300 GL column (GE Healthcare Life Science). This column was chosen for its chemical stability, sample volume range, high resolution, and ability to accommodate the molecular weight of the sample solution. The nanodisc solution was vortexed to homogenize and centrifuged at 14,000 rpm in a benchtop microcentrifuge for 10 min to remove large particles. Approximately 250 µL of nanodisc solution was injected into the column, run through the column connected to ÄKTApure25 with parameters reported in Table 2.1, and eluted in a fraction of 500 µL with the same buffer (20 mM Tris pH 7.8, 100 mM NaCl) as the nanodisc solution was initially in. The run parameters were executed using UNICORN software. The column was washed with one column volume of the buffer solution between each run. The collected fractions were further analyzed using DLS and SDS-PAGE.

Table 2.1. Instrument Parameters for FPLC-SEC Purification

Flow rate	0.5 mL/min
Pressure limit	2.6 MPa
Column volume	23.562 mL
Loop type	Capillary loop
Loop length	0.5 mL

In order to determine the size of the particles in nanodisc solution, the column was calibrated with a mixture of standards: ovalbumin (O), aldolase (A), ferritin (F), and thyroglobulin (T) (GE Healthcare Life Science). The standards were chosen based on

their molecular weight and the Stoke's diameter. Since the nanodisc was predicted to form around the diameter of 10 nm, the standards with Stoke's diameter ranging from 6 to 17 nm were chosen to calibrate the column. 1 mL of mixed standard solution was prepared with concentrations of 4 mg/mL (O), 4 mg/mL (A), 0.3 mg/mL (F), and 5 mg/mL (T). About 250 µL of the mixed standard solution was injected into the column and run with the same flow rate and pressure limit as described above. The chromatogram of a mixture of four standards solution was shown in Figure 2.5a. The elution volume was plotted against the Stoke's diameter of each standard, and the linear-fit equation was reported to be y = 0.0527 x + 0.286 (Fig. 2.5b).

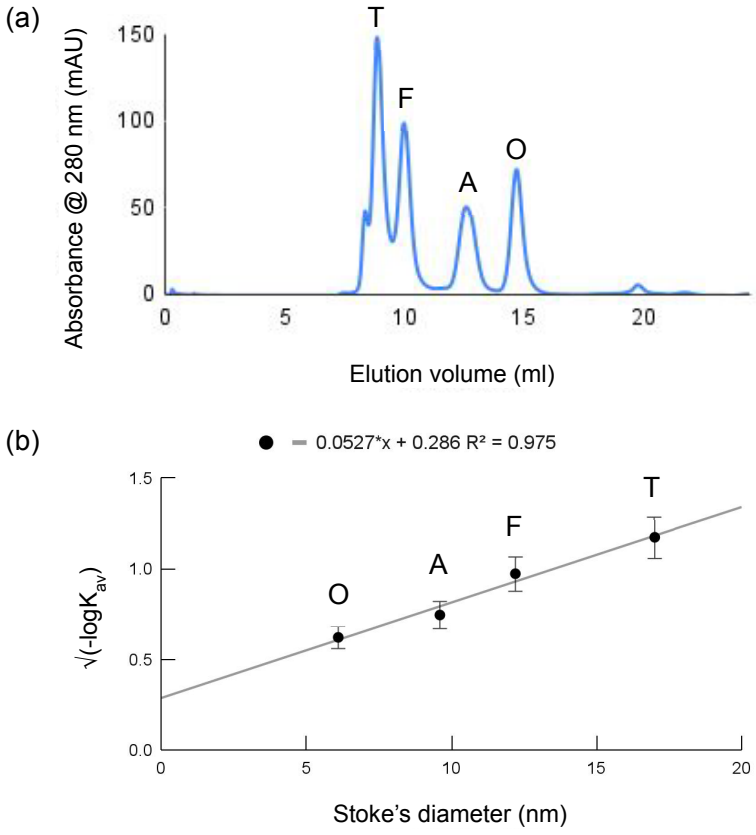

Figure 2.5. Standards Calibration for Stoke's diameter determination of nanodiscs. (a) FPLC-SEC chromatogram of a mixture of four standards: ovalbumin (O), aldolase (A), ferritin (F), and thyroglobulin (T). (b) The elution volume (ml) of the top of each peak in the chromatogram is graphed against the known Stoke's diameter (nm) of each standard. The fit equation is shown with the R^2 value of 0.975.

2.5. Physical Characterization of Nanodiscs via Dynamic Light Scattering (DLS)

Dynamic Light Scattering (DLS) is a technique that can be used to determine the size distribution profile of particles in solution. A monochromatic light source is shown through a polarizer and into a sample (Fig. 2.6). The scattered light then goes through a second polarizer where it is collected by a detector. The diffracted light from all the molecules can either interfere constructively (light regions) or destructively (dark regions). This process is repeated at short time intervals and analyzed by an autocorrelator that compares the intensity of light at each spot over time to determine the average size of the particles.

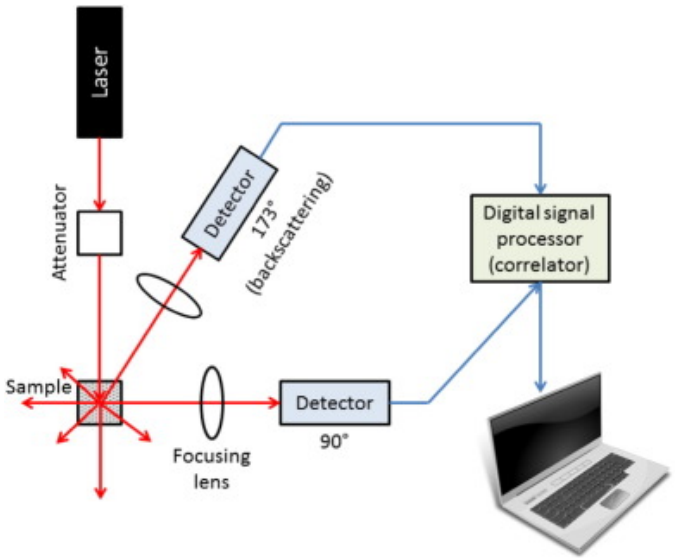

Figure 2.6. Flowchart of DLS data collection. Zeta size of nanodisc samples was measured, and instrument parameters were reported in Table 2.2.

The pre-FPLC nanodisc solution and post-FPLC collected fractions of nanodisc solution were spun at 14,000 rpm in benchtop microfuge for 10 min to remove any large particles from the sample. For post-FPLC collected fractions, only the fractions that show UV absorbance were analyzed. Approximately 500 µL of nanodisc solution was transferred to a semi-disposable cuvette and analyzed. DLS were collected on a Malvern

Zetasizer Nano-ZS and reported as the average of the five measurements. Instrument parameters for DLS and zeta size are reported in Table 2.2.

DLS is sensitive to the size of the particle and reports the intensity based total scattering. For instance, if only 1% of the volume is large particles and the rest are nanodiscs, DLS intensity data might report 50% intensity of nanodiscs and 50% intensity of large particles, just because large particles are so much bigger than the size of nanodiscs. Therefore, % Volumes data were used to plot the size distribution plot of nanodisc samples.

Table 2.2. Instrument Parameters for DLS and Zeta Size measurements

Backscatter mode	173°
Dispersant	water
Temperature	25.0℃
Equilibration time	120 sec
Number of runs	10
Number of measurements	5

2.6. Biophysical Analysis of Nanodiscs via Electron Paramagnetic Resonance Spectroscopy

Site-Directed Spin Label Electron Paramagnetic Resonance (SDSL-EPR) spectroscopy has emerged as a powerful way to study MPs.[6,35,36] SDSL-EPR spectroscopy is especially suited to study MPs because it can provide information on the location and environment of a specific residue on the MPs while in solution, which allows us to study the MPs in their biological condition. This section will briefly outline the basics of EPR and some of the information that can be obtained using SDSL-EPR.

2.6.1. EPR Theory

EPR spectroscopy measures the absorption of microwave radiation corresponding to the energy splitting of an unpaired electron in the presence of a magnetic field. The electron has a magnetic moment, *s*, and spin quantum number, m_s, and occupies one of the two spin states: $m_s = +½$ or $m_s = -½$. In the absence of an external magnetic field, the two spin states have the same energy. In the presence of an external magnetic field (B_0), the magnetic moment aligns itself to the field either parallel ($m_s = -½$, lower energy state) or antiparallel ($m_s = +½$, higher energy state), known as Zeeman splitting (Fig. 2.7).

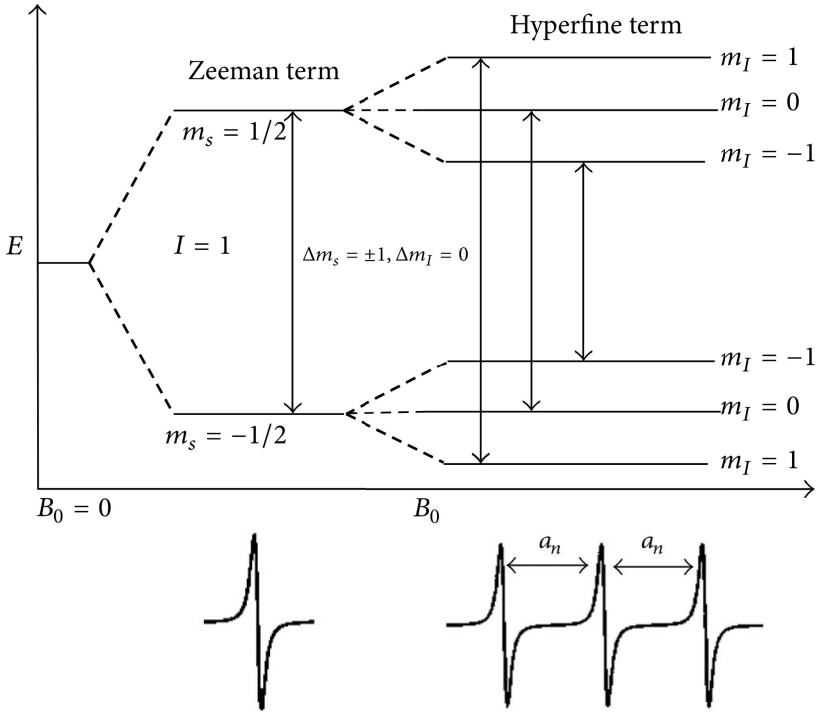

Figure 2.7. Energy level diagram of a free spin-label in solution in the presence of a magnetic field B_0. The energy splitting of an electron due to Zeeman splitting and Hyperfine splitting are shown on the top. EPR spectra in the absence and presence of a ^{14}N nucleus with $I = 1$ hyperfine interaction is shown in the bottom. Taken from Sahu et al., 2018.[35]

The energy difference between the two spin states is proportional to the magnitude of the applied external magnetic field and is described by the equation: $\Delta E = h\nu = g_e \mu_B B_0$, where g_e is the g-factor for the electron, μ_B is the Bohr magneton, and

B_0 is the strength of the magnetic field.[37,38] EPR spectra are generally recorded as the first derivative of the absorbance spectra as it provides better signal to noise ratio.[37,39–41]

If a nearby nucleus to an unpaired electron has a non-zero nuclear spin, such as a nitrogen-14 nucleus with $I = 1$, the electron's spin states can be split again by neighboring nuclei. That interaction is called hyperfine splitting and splits the EPR lines into multiple lines depending on the nuclear spin state. The number of additional energy states corresponds to the nuclear spin of the splitting nuclei in the relationship $2nI+1$, where n is the number of nuclei with the same I. For instance, the splitting pattern of a nitroxide radical of the MTSL spin-label we use, with the radical localizes nitrogen atom is shown in Figure 2.8, The ^{14}N nucleus with $I = 1$ splits the electron spin states into three substates, $m_I = -1, 0, 1$. Only transitions between energy levels with $\Delta m_s = \pm 1$ and $\Delta m_I = 0$ are allowed, so three peaks are observed in the line shape of a nitroxide radical as shown in Figure 2.7.

2.6.2. Site-Directed Spin Label EPR Spectroscopy

In order to study M2 using EPR, we attached a spin-label (MTSL) at a specific site. In order to install the spin-label on M2 protein, a single cysteine mutation is introduced at the site of interest via site-directed mutagenesis. The cysteine sulfhydryl (thiol group) on M2 forms a disulfide linkage to MTSL (Fig. 2.8). This process is called site-directed spin labeling (SDSL), and SDSL-EPR can provide information on the local environment, structure, and proximity of the individual residues, as well as side chain mobility and accessibility to the paramagnetic relaxation agents, such as oxygen.[36]

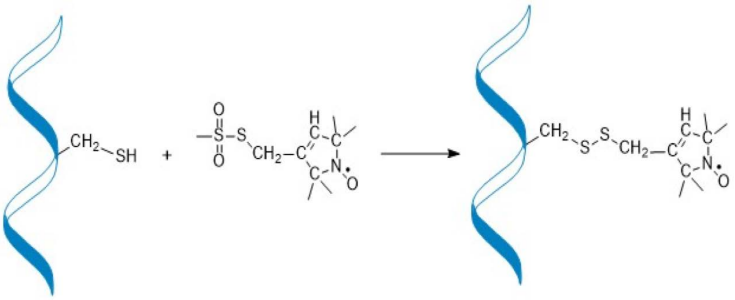

Figure 2.8. Spin labeling reaction of MTSL to cysteine residue on M2 protein. Cysteine sulfhydryl on M2 reacts with thiosulfonate ester on MTSL, forming disulfide linkage.

2.6.3. Continuous Wave (CW) spectrum and Spin Mobility

The spin-label mobility is encoded in the EPR line shape, which is sensitive to rotational motion in the range of 0.1 to 100 nanoseconds. Depending on the rates of the rotational motion, the amplitude and broadness of the line shape can vary (Fig. 2.9). For instance, at fast motion (in solution), the three sharp lines with similar height can be observed. As the motion slows down (bound to protein), the lines broaden and the amplitude decreases. Lastly, for the immobile spin-label in the frozen sample, the conventional, first-derivative spin-label EPR spectrum is shown. A common way to quantitatively express the line shape, and thus a measure of mobility is to calculate the inverse of the central peak width of the CW spectrum (ΔH^{-1}).

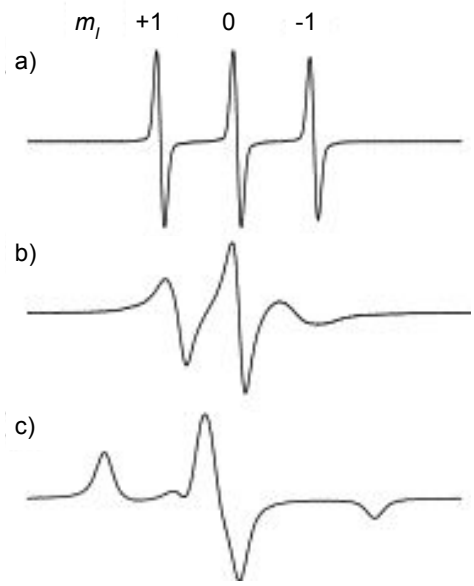

Figure 2.9. The CW EPR spectra of MTSL (a) in solution, (b) bound to residue on α-helix protein, (c) in frozen solution. Adapted from Klug et al., 2008.[36]

2.6.4. Membrane Topology from Accessibility to Oxygen Power Saturation Studies

SDSL-EPR can also provide the spin labeled site's accessibility to paramagnetic reagents through power saturation experiments. Under non-saturating conditions, the height of the spectral lines is in linear relationship with the square root of the microwave power (Fig. 2.10). When high enough power is used, the spin-label cannot relax fast enough to absorb the additional photons, and the increase in height of the spectral lines will decrease. This process is called the saturation of the signal. However, when the paramagnetic relaxation agent is introduced, the relaxation rate of the spin-label increases, and more power is required to fully saturate the signal. The paramagnetic relaxing agent used in this study is oxygen because it is small, hydrophobic, and largely concentrated in the lipid bilayer. Therefore, the spin-label's accessibility to oxygen can be used to determine the depth of the residue on M2 buried in the lipid bilayer. Because the microwave power can fluctuate during the data collection, the natural relaxation rate of the spin-label is collected in the presence of nitrogen to set a baseline because N_2 is not a paramagnetic relaxing agent.

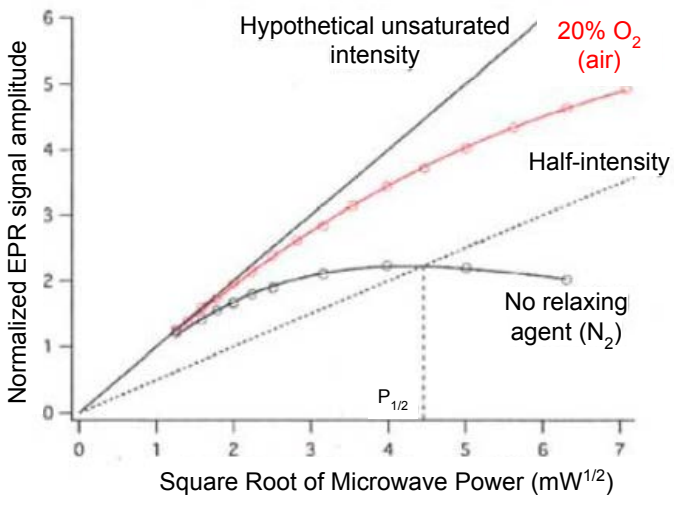

Figure 2.10. Representative oxygen accessibility from power saturation studies. EPR intensity has a linear relationship with the square root of microwave power (black straight line). Half intensity is shown with a dotted line. The EPR signal trend of various microwave powers in the presence of a non-paramagnetic reagent (N_2) is shown with the black curve line and in the presence of a paramagnetic reagent (O_2) is shown with the red curve line.

For oxygen accessibility studies, a sample was placed into a gas permeable TPX tube. To reference the oxygen accessibility data, an experiment was first collected by removing air from the sample by flushing the sample with dry nitrogen gas for 20 min. Next, the experiment was repeated after the sample was left in ambient air for 15 min. EPR spectra were collected at a series of microwave powers. The instrument parameters for power saturation are listed in Table 2.3. The EPR spectra collected from power saturation experiments were processed using Igor Pro 8 software and the power at which line amplitude is half of the theoretical unsaturated amplitude, $P_{1/2}$, in the presence of N_2 and O_2 were calculated with a 95% confidence interval. The difference in $P_{1/2}$ between the spin-labeled sample with no paramagnetic relaxation agent and that with paramagnetic relaxation agent gives you the spin-label's accessibility to the paramagnetic relaxation agent. In other words, $\Delta P_{1/2}$ (O_2) value can provide you information about the membrane accessibility of the spin-labeled residue on the M2 protein.

Table 2.3. Instrument Parameters for EPR CW and Power Saturation experiments

CW spectrum (Magnetic Field Sweep)		
Center field	3480 G	
Sweep width	150 G	
Sweep time	41.943 s	
Sample g-factor	2	
Modulation frequency	100.0 kHz	
Modulation phase	0.0	
Modulation amplitude	6.825	
Time constant	20.48 ms	
Power Saturation (Microwave Power Sweep)		
Gases	Nitrogen	Oxygen
Start attenuation	7 dB	2 dB[a]/6 dB[b]
Increment	2 dB	1 dB
Number of points	8	19[a]/16[b]
Settling time	500 ms	

[a]For samples with high accessibility to oxygen, such as sites 43 and 57 of M2, which are in the transmembrane region and buried in the membrane, more power is needed to fully saturate the signal.
[b]For samples with moderate accessibility to oxygen, such as sites 68 and 82 of M2, which are in the amphipathic and C-terminal region, respectively, moderate power is enough to fully saturate the signal.

Chapter 3: Development of Nanodiscs Membrane System for Biophysical Studies on M2

3.1. Strategy to Optimal Conditions for Making Nanodiscs for M2s

Membrane protein containing discoidal lipid bilayer membranes called nanodiscs are prepared by combining bilayer forming lipids, a membrane scaffold protein (MSP) and a detergent solubilized membrane protein of interest. The detergent is then removed, and the MP-nanodiscs spontaneously form. The molar ratio of M2 to MSP to lipid is essential to be optimized for the protein of interest in order to obtain the most homogeneous sample with the highest yield. The rationale for choosing each component as well as the molar ratio of each component was described in the following subsections.

3.1.1. Choice of lipid

We used 4:1 POPC/POPG bilayers because M2 was shown to be functional in this membrane environment using both an *in vitro* budding assay and channel electrophysiology.[29,31] Furthermore, a large body of previous work used POPC:POPG bilayers, so there was published work to compare our data to.[5,6,26,28,30,33]

3.1.2. Choice of MSP

A range of different MSP constructs have been used in the literature to make nanodiscs. Two of the MSP constructs most commonly used in nanodisc applications are MSP1D1 and MSP1E3D1, which form nanodiscs that are approximately 10 and 13 nm, respectively (Fig. 3.1a-c).[42] The surface area of transmembrane helix is estimated to be 80 Å,[10] and therefore, since our goal is to construct a nanodisc that allows for the incorporation of one M2 homotetramer per nanodisc, it makes sense to use a slightly smaller nanodisc system (Fig. 3.1b, c). Therefore, MSP1D1 is the construct used in this

study to make nanodiscs. Commercially obtained MSP1D1 (Cube Biotech Inc., Wayne PA) was used in the first set of trials. Due to the high cost and impurities present in the commercial MSP1D1, plasmid MSP1D1 (under KanR control) was overexpressed and purified (see Materials and Methods). All the data presented in this study were made using MSP1D1 expressed and purified in our lab (Fig. 2.4).

(a)

```
MSP1D1          GHHHHHHHHDYDIPTTENLYFQGSTFSKLREQLGPVTQEFWDNLEKETEGLRQEMSKDLEE 60
MSP1E3D1        GHHHHHHHHDYDIPTTENLYFQGSTFSKLREQLGPVTQEFWDNLEKETEGLRQEMSKDLEE 60

MSP1D1          VKAKVQPYLDDFQKKWQEEMELYRQKVEPLRAELQEGARQKLHELQEKLSPLGEEMRDRA 120
MSP1E3D1        VKAKVQPYLDDFQKKWQEEMELYRQKVEPLRAELQEGARQKLHELQEKLSPLGEEMRDRA 120

MSP1D1          RAHVDALRTHLAPYSD---------------------------------------- 136
MSP1E3D1        RAHVDALRTHLAPYLDDFQKKWQEEMELYRQKVEPLRAELQEGARQKLHELQEKLSPLGE 180

MSP1D1          ----------------------ELRQRLAARLEALKENGGARLAEYHAKATEHLSTLSEK 174
MSP1E3D1        EMRDRARAHVDALRTHLAPYSDELRQRLAARLEALKENGGARLAEYHAKATEHLSTLSEK 240

MSP1D1          AKPALEDLRQGLLPVLESFKVSFLSALEEYTKKLNTQ                         211
MSP1E3D1        AKPALEDLRQGLLPVLESFKVSFLSALEEYTKKLNTQ                         277
```

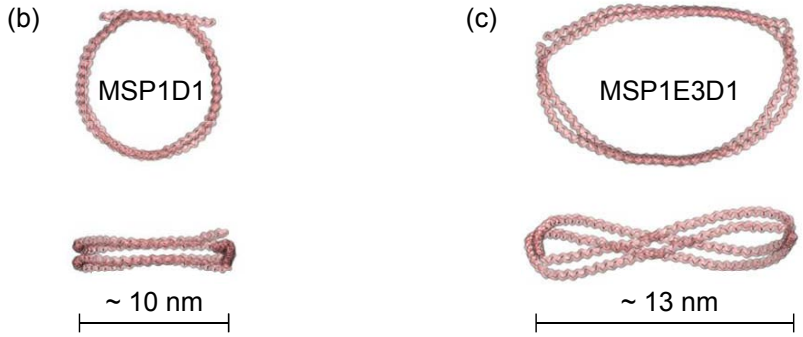

Figure 3.1. Membrane scaffold protein constructs. (a) Sequences of two commonly used membrane scaffolid proteins (MSP1D1 and MSP1E3D1) used for forming nanodiscs. (b) Models of MSP1D1 and (c) MSP1E3D1 constructs. The representative models are adapted from Kjølbye et al., 2021.[43]

3.1.3. Systematic Change in Ratios of Nanodisc Components

Ritchie et al. optimized the MSP1D1 to lipids molar ratio for different types of lipid compositions and found that 1:65 was optimal for solution for POPC lipids.[12] Bayburt et. al first figured out that each nanodisc is made up of 2 strands of MSP. M2 is a

homotetramer that forms a proton channel in liposomes.[8,11] The molar compositions of M2 channel, MSP1D1, and lipids that will be prepared are 1:2:130, 1:5:325, and 1:20:1300. The three compositions are described as 1:2, 1:5, and 1:20 below.

3.2. Nanodisc Preparation Procedure

The overview of the nanodisc preparation procedure is described in Scheme 3.1.

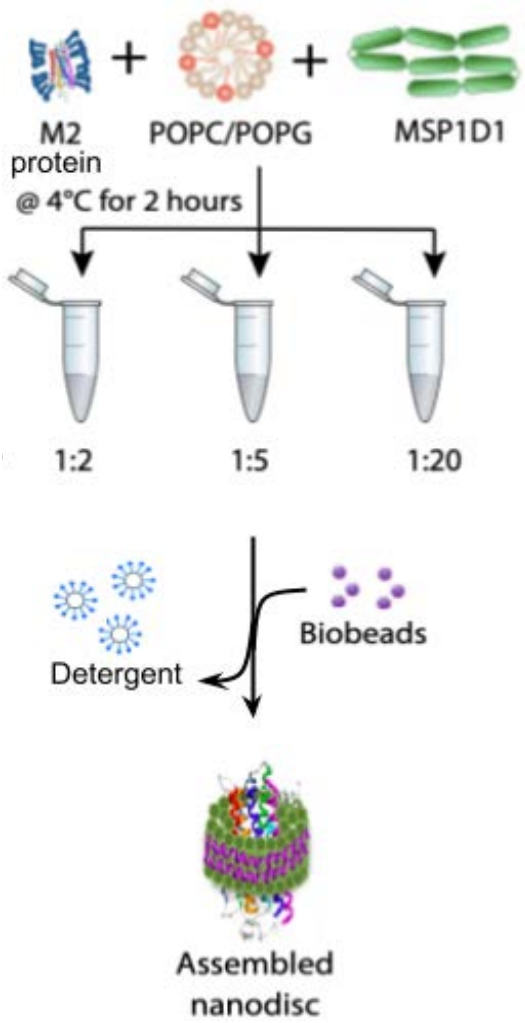

Scheme 3.1. Flowchart of nanodisc preparation tailored for full length M2 protein. Molar ratios of M2 tetramer:MSP1D1 of 1:2, 1:5, and 1:20 were used to make nanodiscs. The ratio of MSP1D1 to lipid was kept the same to be 1:65 for all molar ratio samples. 4:1 POPC/POPG is the lipid composition used. MSP1D1 is the membrane scaffold protein used. M2, POPC/POPG, and MSP1D1 are in octylglucoside (OG) detergent solution. Biobeads are the absorbent used to remove the detergent residue, and are equilibrated in 20 mM Tris pH 7.8, 100 mM NaCl.

M2 was purified and solubilized in OG solution (see Materials and Methods for detail). 4:1 POPC:POPG was dissolved in the 200 mM sodium cholate buffer. MSP1D1 was purified and solubilized in 20 mM Tris pH 7.8, 100 mM NaCl (see Materials and Methods for detail). For optimization of nanodiscs for M2, purified M2 WT proteins (A/Udorn/307/1972 (H3N2)) were used (Fig. 2.1). For biophysical studies with EPR spectroscopy, site-directed spin-labeled M2 proteins were used (Fig. 2.1). For three sets of molar ratios, appropriate amounts of each component for nanodisc were combined and incubated for 2 hours at 4°C. A degassed slurry of hydrophobic polystyrene beads (Biobeads SM-2, Bio-Rad) in 20 mM Tris pH 7.8, 100 mM NaCl was added in aliquots of 50 µL over a period of 3 hours and incubated for additional 8-12 hours to facilitate the removal of detergent. Biobeads were removed, and the nanodisc solution was filtered through 0.45 µm filter paper. The filtered nanodisc solution was characterized by DLS before and after purifying through the FPLC column.

3.3. Physical Characterizations of Nanodiscs using DLS and FPLC-SEC

The nanodisc samples of three molar ratios were characterized the size exclusion chromatography method over the Superdex 200 increase 10/300 GL column to separate the M2-nanodiscs from empty nanodiscs. The column was calibrated with standards of various sizes (see Methods and Materials for details), 250 µL of each sample was injected, and absorbance peak shapes and elution volumes were analyzed. The pre- and post-purified nanodisc samples were analyzed using DLS to determine the size distribution of the samples to assess the purification.

3.3.1. Size distribution of nanodisc samples via DLS

The DLS size distribution plots of the pre-purified and post-purified nanodisc samples show that the size of most particles in solution decreases with increasing amount of MSP1D1. The Stoke's diameter of those particles are determined to be 11.9 (±0.2) nm for 1:2 sample, 10.6 (±0.6) nm for 1:5 sample, and 8.5 (±0.2) nm for 1:20 sample (Fig. 3.2). The shift is consistent with a population of empty nanodiscs, which are smaller in size than M2-nanodiscs.

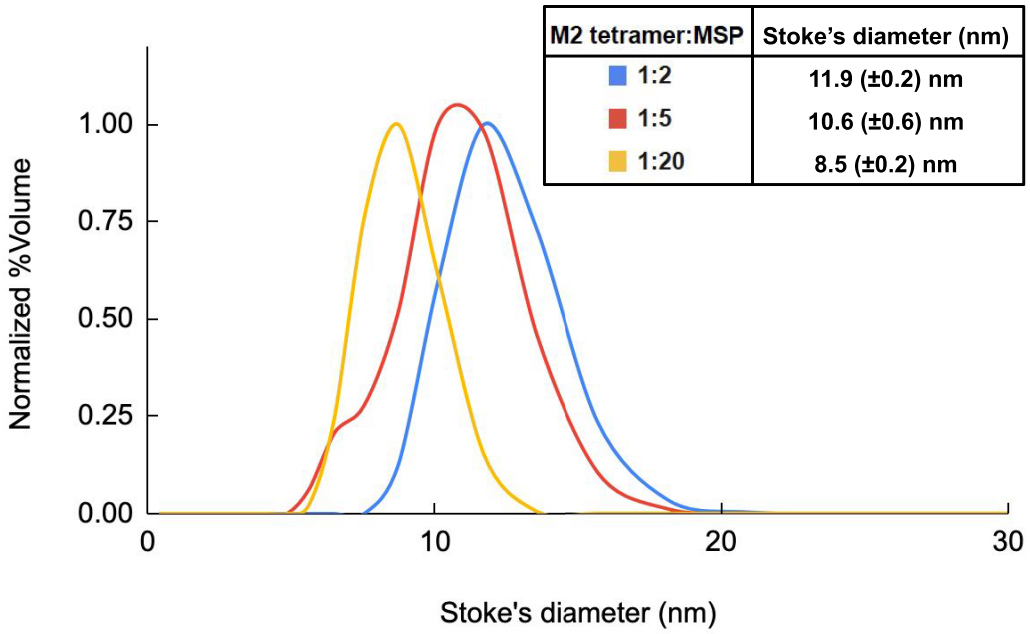

Figure 3.2. DLS size distribution of pre-FPLC 1:2, 1:5, 1:20 (M2 tetramer:MSP1D1) sample solutions. The Stoke's diameter is reported in the legend.

3.3.2. Purification and Size determination of nanodisc samples via FPLC-SEC

The top peak of the FPLC-SEC chromatogram shifts to the right as the molar ratio of MSP1D1 to M2 tetramer increases (Fig. 3.3a). It suggests that a large portion of the sample solution comprises smaller particles in the 1:20 sample compared to the other two ratios, which assumes empty nanodiscs are not resolved from M2 containing nanodiscs. Additionally, a minor peak near an elution volume of 15 mL becomes more prominent in

the 1:20 sample, which implies that it is more heterogeneous compared to 1:2 and 1:5 samples. The Stoke's diameter of each molar ratio sample was calculated from the elution volume of the top of the peak in the chromatogram, using the calibration equation created using a mixture of four standards (See Material and Method, Fig. 2.5). The Stoke's diameters are calculated to be 11 (±2) nm, 10 (±2) nm, and 8 (±2) nm for 1:2, 1:5, and 1:20 samples, respectively.

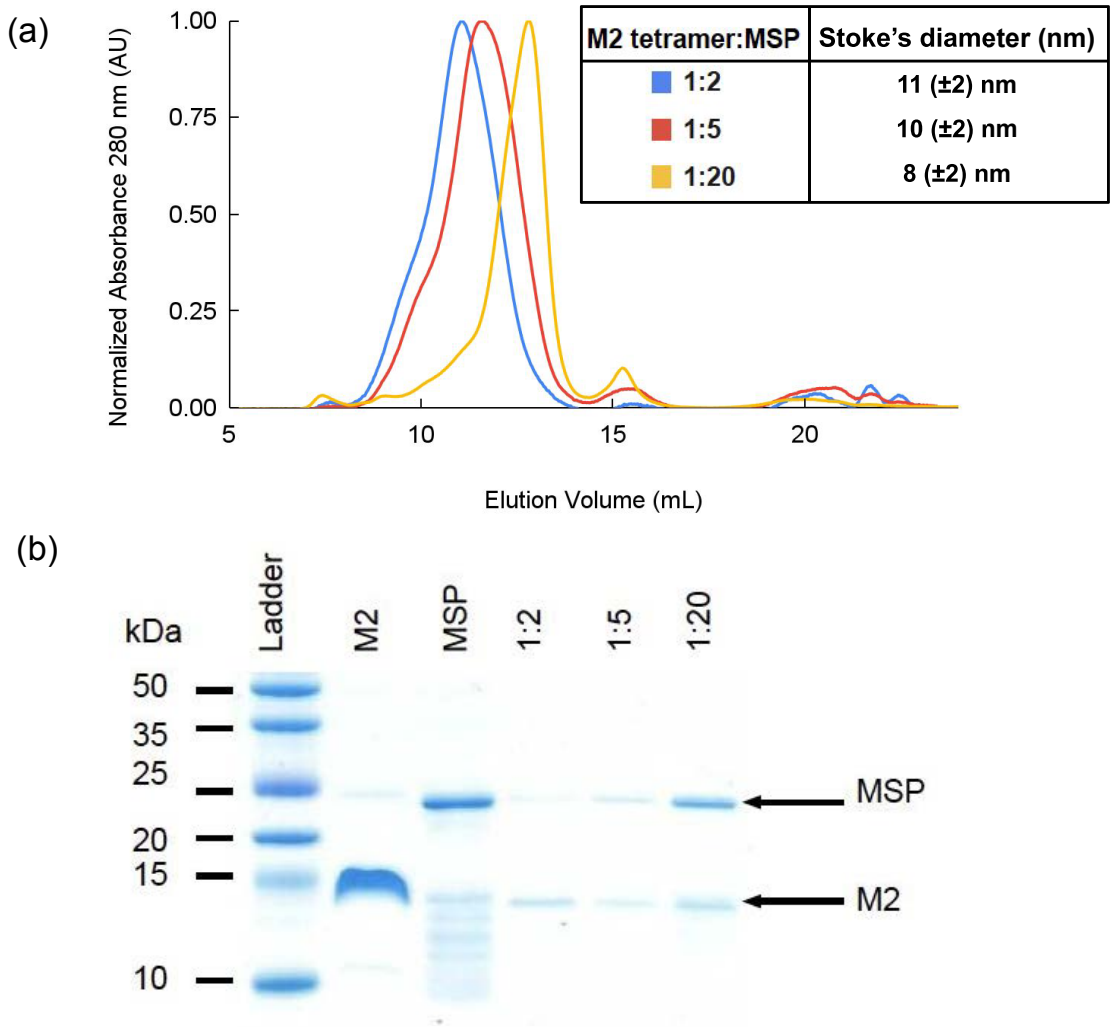

Figure 3.3. Physical characterization of nanodisc**.** (a) FPLC-SEC chromatogram. The calculated Stoke's diameters are reported. The protein content of the nanodiscs from the top of each peak in the chromatogram is shown in SDS-PAGE gel (b), indicating that the nanodisc contains both MSP1D1 and M2 protein, and is not simply aggregates of one or the other. The samples were prepared according to **Scheme 3.1**. NOTE: in the M2 lane, an intense band corresponding to the monomer (~12 kD) as well as a faint band corresponding to dimer (~24 kD) are visible.

The identity of protein content in each molar ratio nanodisc sample was determined using SDS-PAGE gel. The fractions corresponding to the top of the peak, collected from the FPLC column, of each molar ratio were run on SDS-PAGE gel. The bands in Figure 3.3b confirm that the absorbance observed in FPLC chromatograms is indeed due to both M2s and MSP1D1, and not aggregates of one or the other.

A collection of DLS, FPLC-SEC, and SDS-PAGE gel suggests that one M2 channel (four M2 monomers or one M2 homotetramer) is incorporated into one nanodisc (two MSP1D1 monomers), and that excess MSP1D1 molecules result in empty nanodisc (Fig. 3.2 and Fig. 3.3). Therefore, higher amount of empty nanodiscs seem to be present in the 1:20 sample, based on the size analysis by DLS and FPLC-SEC (Fig. 3.2 and Fig.3.3a). In light of producing a size-controlled nanodisc solution with little or no empty nanodiscs, we have concluded that 1:2 sample's composition will be used for further analysis since it produces a high homogeneous sample and uses less amount of purified M2 protein and MSP1D1. It is preferable since the purification process for MSP1D1 is time consuming and costly.

Chapter 4: Comparison of Dynamic Properties and Membrane Topology of M2 in Liposomes and Nanodiscs

Membrane proteins have been shown to change conformations and dynamics depending on the hydrophobic environment provided by a membrane mimic.5 Two properties, mobility and membrane topology were measured for M2 in both nanodiscs and liposomes to see if they were similar.

4.1. Spin-labeled Sites on M2

We selected four sites to spin-label across the M2 protein: L43, H57, V68, and S82. The positions include the end of the transmembrane helix, the beginning and end of the amphipathic helix and a site in the flexible, highly mobile C-terminal tail (Fig 1.4 and Fig. 2.1). These four sites had been studied previously in liposomes and have been shown to have properties characteristic of the region of the protein in which they are located. SDSL-EPR spectroscopy was used to measure EPR line shapes and oxygen power saturation data for the four sites of M2 reconstituted into nanodiscs and liposomes.

4.2. Spin-labeled M2's Mobility in Nanodiscs and Liposomes

X-band CW spectra of four spin-labeled M2 constructs in nanodiscs show a typical line shape for membrane proteins (Fig. 2.9),[36] and they have a similar trend as those in liposomes (Fig. 4.1a-d). That suggests that the M2 tetramer in nanodiscs presents the similar conformation as that in liposomes. The width of the CW spectrum's central peak of site 43 is broadest since it is in the transmembrane region, which is most buried in the membrane. The central peak becomes sharper as the location of the site moves

farther away from the membrane. Thus, the CW spectrum's central peak of site 82 is the sharpest since it is in the dynamic C-terminal region. The similarity in EPR line shapes between the nanodiscs and liposomes is consistent with the presence of MSP1D1 not perturbing the conformation observed in liposomes.

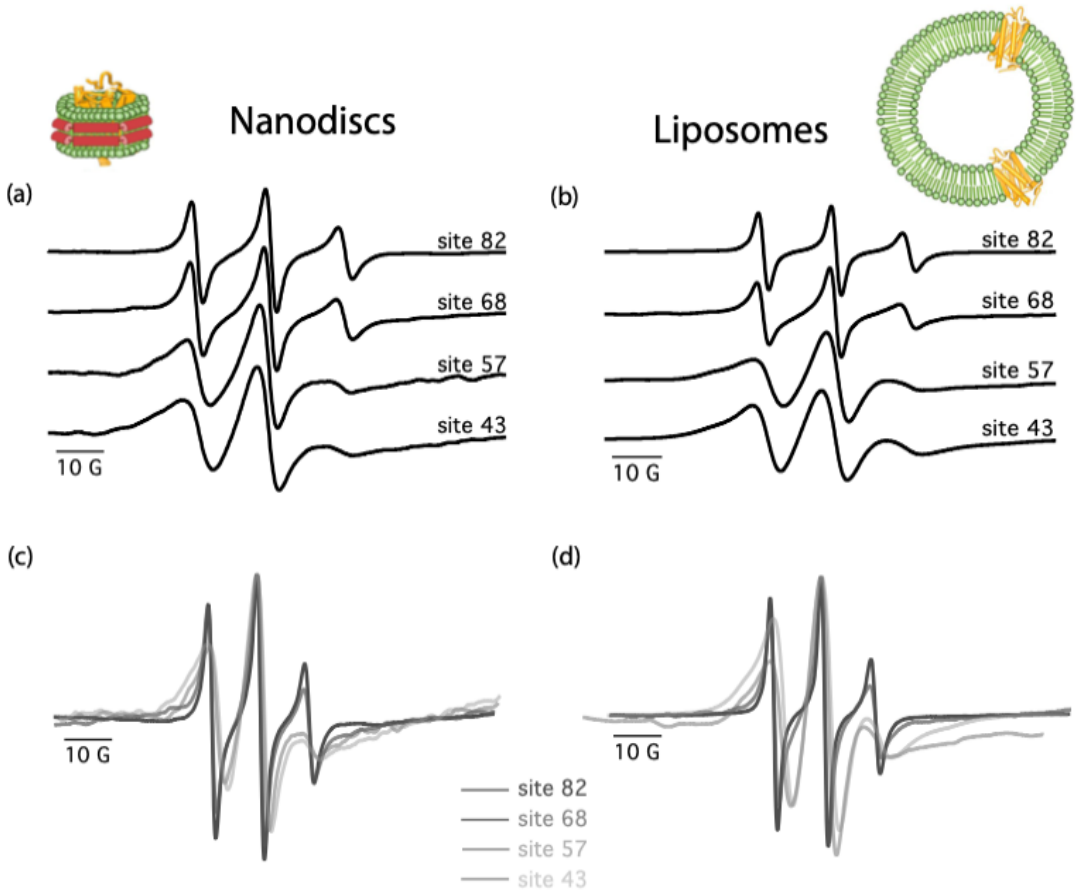

Figure 4.1. EPR line shapes of site-specific, spin-labeled M2s in nanodiscs and in liposomes. X-band continuous wave (CW) spectra of four spin labeled sites in nanodiscs (a) and in liposomes (b). Overlay CW spectra of nanodiscs are shown in (c) and of liposomes are shown in (d).

ΔH^{-1} provides information about the spin-label mobility of M2 in membrane mimics; the greater the ΔH^{-1}, the more mobile the probed residue is. The spin-label mobility trend of M2 in nanodiscs is similar to that in liposomes (Fig. 4.2a, b). ΔH^{-1} values of site 82 in both membrane systems are similar enough to suggest that spin-labeled M2 tetramers have a similar local environment that allows similar motional

freedom. However, ΔH^{-1} values of sites 43, 57, and 68 in nanodiscs are slightly higher than ΔH^{-1} values of the same three sites in liposomes, with site 68 having the largest difference.

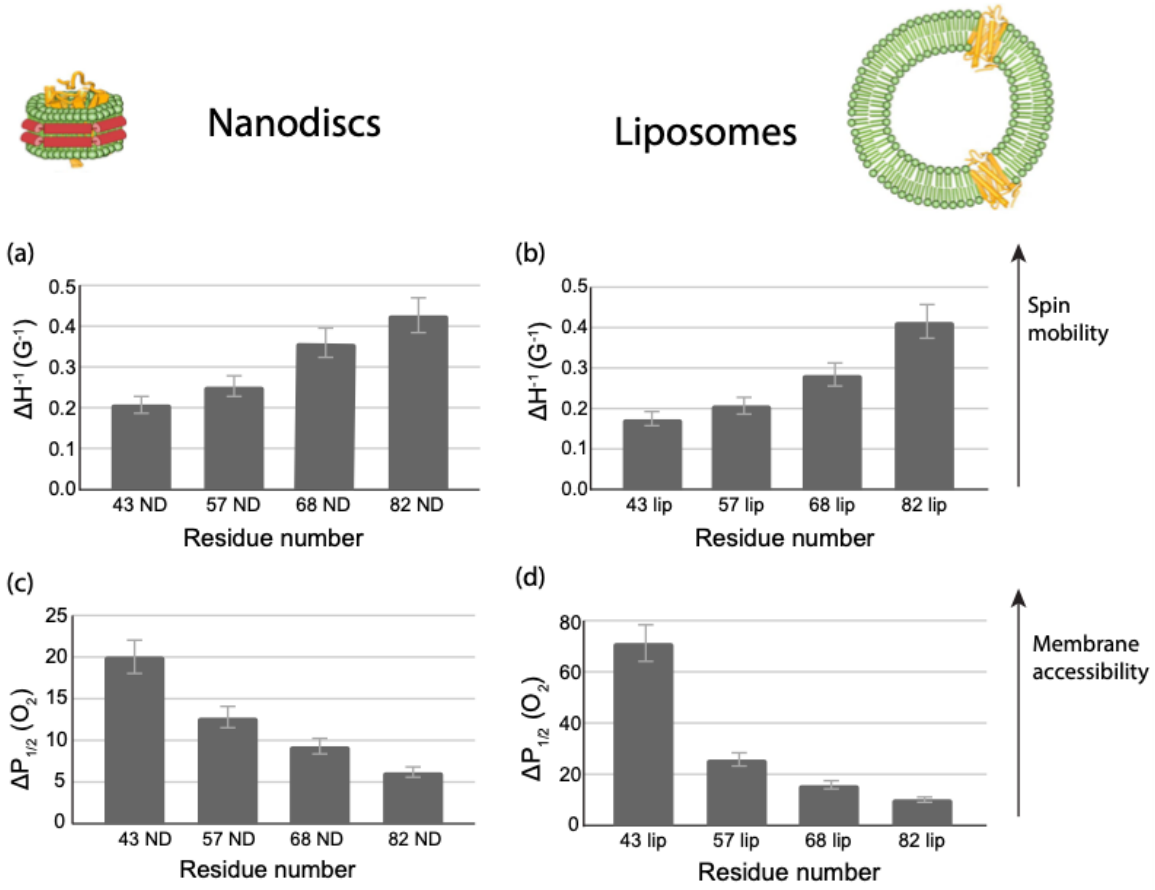

Figure 4.2. **Mobility and Membrane Topology of M2 in nanodiscs and in liposomes**. Mobility parameter for specified sites in M2 (a) in nanodiscs and (b) in liposomes. Oxygen accessibility for specific sites on M2 (c) in nanodiscs and (d) in liposomes. ΔH^{-1} is calculated from the CW spectra of each residue number. $\Delta P_{1/2}$ is calculated using Igor Pro 8 software. $\Delta P_{1/2}$ (O_2) is the difference between $\Delta P_{1/2}$ (N_2) and $\Delta P_{1/2}$ (O_2). ND: nanodiscs, lip: liposomes.

4.3. Membrane Topology of Spin-labeled M2 in Nanodiscs and Liposomes

The oxygen accessibility of the probed residue to oxygen can be quantified by calculating $\Delta P_{1/2}$ (see Materials and Methods for details). The greater the $\Delta P_{1/2}$, the more buried the probed residue is in the membrane. Oxygen is a small, hydrophobic molecule,

and they preferentially partition into the lipid bilayer and not remain in the aqueous phase, so $\Delta P_{1/2}$ can also be used to determine the membrane depth of the spin-labeled site on M2. The $\Delta P_{1/2}$ trend of selected spin-labeled sites of M2 tetramer in nanodiscs is similar to that in liposomes (Fig. 4.2c, d). $\Delta P_{1/2}$ (O_2) was obtained from the difference between $P_{1/2}$ (N_2) and $P_{1/2}$ (O_2). In both nanodiscs and liposomes, site 43 is most buried in the membrane and the protein extends in the aqueous media as you most towards the C-terminus.

Although the trends over the sequence are the same between nanodiscs and lipsomes, there is a difference in magnitude between $\Delta P_{1/2}$ (O_2) values in nanodiscs are significantly smaller than those in liposomes. We hypothesize that the presence of the MSP surrounding the lipid bilayer in nanodiscs allows for more water to penetrate the bilayer making it less hydrophobic. This situation leads to less hydrophobic oxygen partitioning in the bilayer. The decrease in paramagnetic oxygen concentration within the nanodiscs thus leads to less power needed to saturate the signal and smaller $\Delta P_{1/2}$ (O_2) value.[33,34]

Chapter 5: Impact of Antiviral Drug Binding on M2 in Nanodiscs and Liposomes

Conformational exchange is an essential property of the M2 protein. For example, previously published data indicates that there are conformational changes in M2 induced by antiviral drugs.[28] Thus, another goal of this thesis was to see if conformational changes previously seen in liposomes can be observed in nanodiscs.

The adamantanes are a class of antiviral drugs that includes amantadine and rimantadine (Fig. 5.1a). They bind to the M2 proton channel (M2 tetramer) of influenza A viruses, thereby inhibiting the viral entry or viral budding process in the viral life cycle (Fig. 5.1b). The impact of drug binding of M2 in both nanodiscs and liposomes was studied using SDSL-EPR.[28]

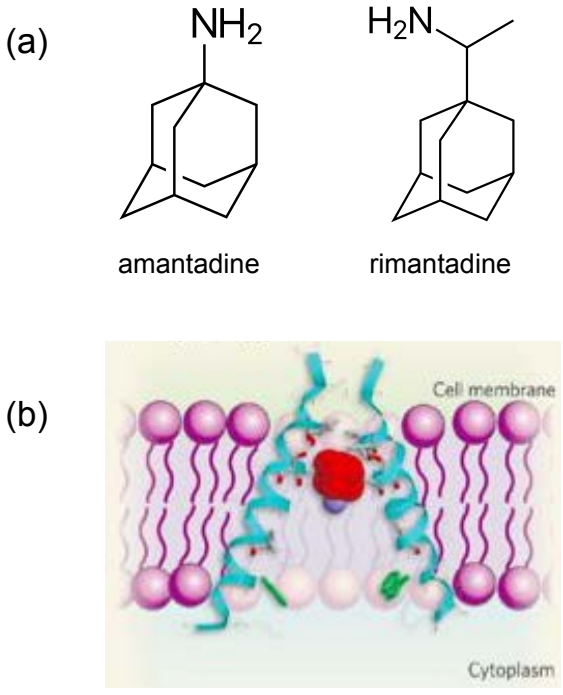

Figure 5.1. Adamantanes antiviral drugs binding to M2 proton channel. (a) Structures of amantadine (left) and rimantadine (right). (b) X-ray structures of the M2 proton channel bound to amantadine. Amantadine is shown in red and two M2 monomers of the channel is shown in blue.

5.1. Introduction

In previous work, site 43 was shown to have significant changes in dynamics and oxygen accessibility upon rimantadine binding to M2 embedded in liposomes.[28] Rimantadine was used in this study because the previous study showed that the largest conformational change was observed in the addition of rimantadine.[28]

5.2. Preparation of M2 tetramer in Membrane Systems with Rimantadine

Rimantadine drug stock solution was prepared in trifluoroethanol, and appropriate volumes were aliquoted into glass vials for M2 tetramer to drug molar ratio of 1 to 10. Trifluoroethanol was removed under a gentle stream of nitrogen gas overnight. Preformed proteoliposomes and nanodiscs were added to the drug films, vortexed, and incubated for 24 hours at room temperature. The EPR CW spectra and power saturation data were collected as described in the Materials and Methods section.

5.3. Site 43 in the Presence of Rimantadine Shows Slight Decrease in Mobility and in Membrane Accessibility

The EPR CW line shapes of site 43 labeled M2 tetramer in nanodiscs and liposomes show that peaks' width slightly broadens after the addition of rimantadine (Fig. 5.2a, b). ΔH^{-1} values of site 43 with drug also show a slight decrease, compared to that without drug in both nanodiscs and liposomes (Fig. 5.2c). That suggests that there is in fact a decrease in spin mobility, which might be an indicator of drug binding to M2 tetramer in both membrane systems. Oxygen power saturation data for site 43 in nanodiscs and liposomes both show a decrease in the presence of rimantadine (Fig. 5.2d).

The site 43 proteoliposomes with drug was collected by previous Howard lab member, Aaron Holmes, 2017.

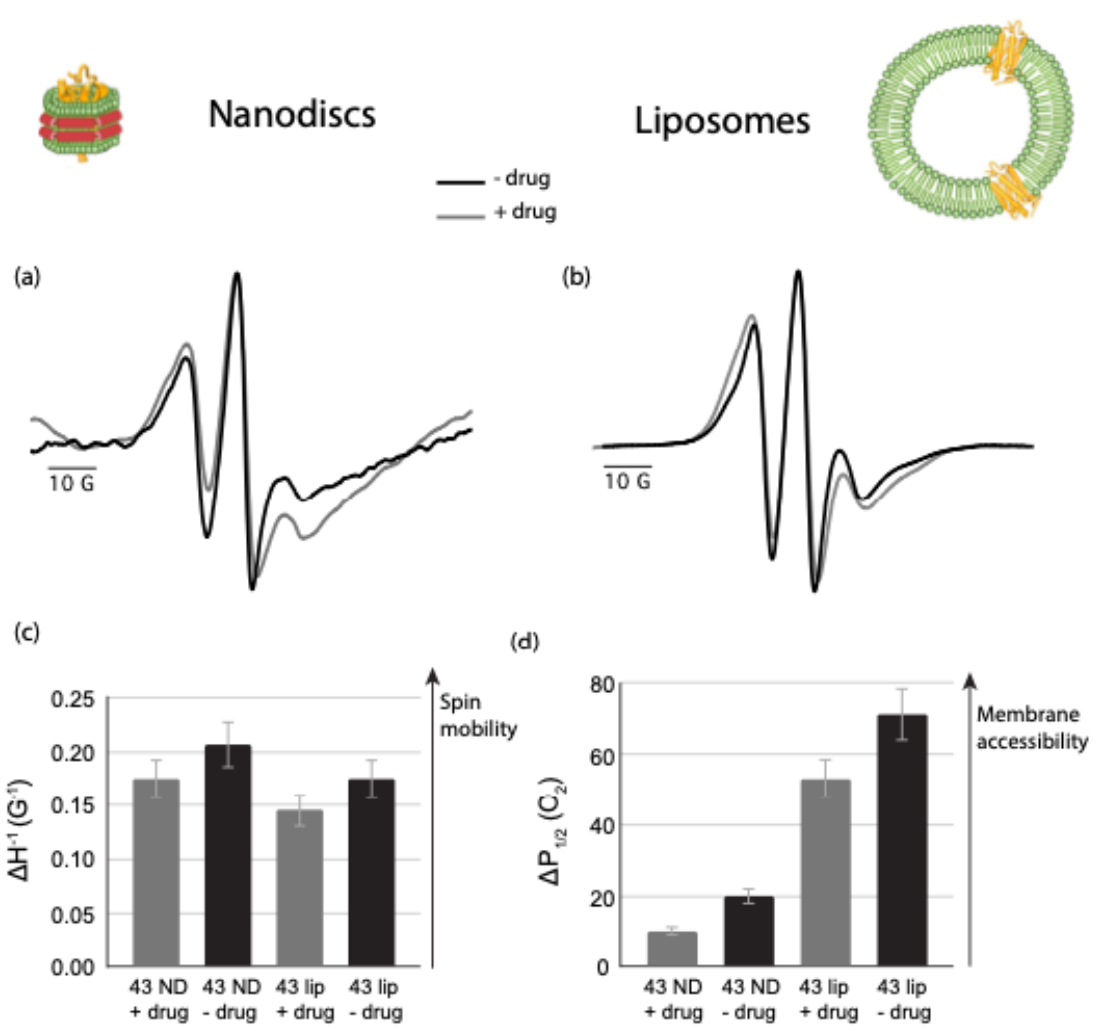

Figure 5.2. Antiviral drug effect on the conformation and dynamic of spin labeled M2 proteins. (a) X-band CW spectra of site 43 labeled M2 (a) in nanodiscs with (gray) and without (black) drug, (b) in liposomes with (gray) and without (black) drug. (c) M2's mobility in nanodiscs and liposomes with (gray) and without (black) drug. (d) M2's membrane accessibility in nanodiscs and liposomes with (gray) and without (black) drug.

Chapter 6: Conclusion and Future Directions

6.1. Conclusions

The goal of this thesis was to explore the potential of using nanodiscs for biophysical studies of membrane-bound M2 protein. Nanodiscs offer advantages over the other membrane mimics used widely in M2 literature.[5,6,17,26] Nanodiscs provide a bilayer environment with access to both sides of the bilayer and are smaller than other well established bilayered, spherical, sealed liposomes whose size provides challenges for some biophysical methods.[2,7]

The literature has shown that the formulation of nanodisc composition is not a one-size-fits-all for membrane proteins.[1,10,12] Instead, the choice of lipids and molar ratios of components needs to be varied to find conditions that lead to homogeneous and stable samples. For example, this thesis' reports demonstrated that a molar ratio of 1:2 (M2 tetramer:MSP1D1) forms a homogeneous and stable preparation of M2-nanodiscs. SDS-PAGE gels were used to look at the protein content of FPLC-SEC fractions and confirmed that the contents in the nanodiscs were a mixture of M2 proteins and MSP1D1, and not aggregates of M2s or MSP1D1. In addition to homogeneity and stability, we wanted to address the question whether the conformation and dynamics of M2 in nanodiscs was physiologically relevant. Electrophysiological assays to probe M2's role as a proton channel[26] and budding assays to demonstrate M2's role as a fission facilitator can be done in liposomes.[45] Both these assays capitalize on liposomes being sealed spheres with a well-defined interior. Conformation and dynamics under conditions that maintain function provide evidence that the published liposome conformation data is functionally relevant. The electrophysiological and budding assays are not viable with

nanodiscs. Thus, in an attempt to show nanodiscs provide an environment that could support a functionally relevant environment, we used the conformations already determined in liposomes as a touchstone to show that nanodiscs are a good model membrane. Both our nanodiscs and liposomes are made up of a bilayer with the same lipids so we hypothesized that they should provide a similar hydrophobic environment for M2. However, we wanted to confirm that the MSP proteins that provide the bilayer belt in nanodiscs were not perturbing the M2 structure.

To compare conformational and dynamic properties of M2 in nanodiscs to those observed in liposomes, we used SDSL-EPR. The EPR experiments of four key spin-labeled M2 sites using nanodisc as the model membrane show similar trends in spin mobility and membrane accessibility to those published for M2 reconstituted into liposome membranes. Although the patterns of mobility and oxygen accessibility of spin-labeled sites between different regions of the protein were the same between nanodiscs and liposomes, the absolute magnitudes of the oxygen accessibility differ. In particular, the oxygen accessibility for liposomes was higher for all sites. This is intriguing given the similarity in magnitudes of mobility factors which suggest the conformation, dynamics, and membrane topology are not different between nanodiscs and liposomes. We hypothesize that the difference in oxygen accessibility is linked to a different bilayer distribution of oxygen in the nanodiscs than in the liposomes. An exploration of this hypothesis is proposed in future studies.

Intense attention has been paid to conformational shifts induced in M2 upon the binding of adamantane drugs.[28] To test whether the conformational changes already observed in liposomes would also be observed in nanodiscs, we compared the impact of

drug binding in nanodiscs to drug binding in liposomes using SDSL-EPR. A spin-label placed at a M2 position near the drug binding site demonstrated a decrease in mobility and membrane accessibility in nanodiscs in a similar fashion as was observed for M2 embedded in liposomes.

6.2. Future Directions

As stated at the beginning of the thesis, a key motivation for working on nanodiscs was to study the interaction of M2 with its many known binding partners. In particular, our group has a particular interest in matrix protein 1 (M1) that has been proposed to bind to the C-terminal domain of M2 and plays an important role in the formation of new viruses. Despite indirect evidence for M2-M1 binding proteins, there is no atomic level demonstrating their interaction or crystal structure of the binding of the two proteins. A lack of unidirectional insertion of M2 into liposomes bilayers means that at least a portion of the M2 proteins in a liposome has their C-terminus of M2 stuck inside the liposome interior where it is obscured from interaction of M1. In nanodiscs both sides of the membrane are accessible to binding. The ability to study M2 in nanodiscs opens up the possibility of a wide range of studies.

In order to use EPR power saturation studies to probe membrane topology, a better understanding must be had of the distribution of paramagnetic oxygen in the bilayers of nanodiscs versus liposomes. Previously, the Howard lab demonstrated that the addition of cholesterol changes how oxygen partitions into a bilayer.[46] A similar strategy could be done on nanodiscs. One can place spin-labels at defined depths within a bilayer and measure oxygen accessibility using the power saturation methods described in the

Materials and Methods section of this thesis. Lipids with spin-label covalently bound at different positions on the lipid chain are commercially available. Since the spin-label depths should be the same in the POPC:POPG bilayers found in both nanodiscs and liposomes, any change in oxygen accessibility could instead be from differing lipid packing induced by the MSP belt. Spin-labeled lipids can be incorporated into lipid bilayer to determine the oxygen accessibility of the bilayer. For example, see the labeled membrane probes shown below.

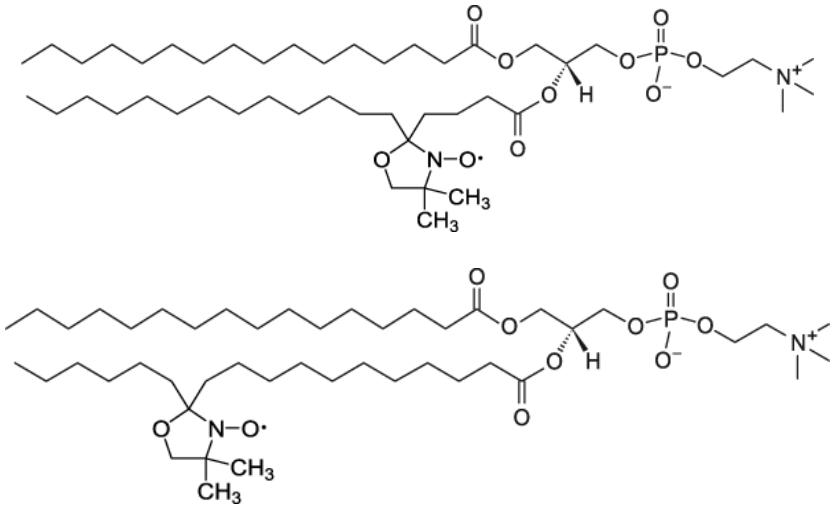

Figure 6.1. Structure of Spin-labeled lipids. 16:0-5 Doxyl PC (top) and 16:0-12 Doxyl PC (bottom) can be used to probe oxygen concentration at different depths.

Acknowledgements

I would like to thank Scout Hayashi for her support and advice throughout this project. I wish her the best of luck in her future biochemistry career. I would also give my gratitude towards Tyrique Arthur for being my best partner in nanodisc optimization procedure. I wish him the best of luck in his future project as well as in his research over the coming summer. I am also grateful for Caleb Porter's effort in modifying the purification of MSP protocol, which makes the nanodisc preparation a lot smoother.

Lastly, my greatest gratitude goes to Dr. Kathleen P. Howard for her endless support and guidance ever since I joined the lab. I would like to thank her for being there for me through the ups and downs that college can bring and through the hard time due to Covid. Words cannot express how thankful I am to have her as my advisor.

References

(1) Nath, A.; Atkins, W. M.; Sligar, S. G. Applications of Phospholipid Bilayer Nanodiscs in the Study of Membranes and Membrane Proteins. *Biochemistry* **2007**, *46* (8), 2059–2069. https://doi.org/10.1021/bi602371n.

(2) Mineev, K. S.; Nadezhdin, K. D. Membrane Mimetics for Solution NMR Studies of Membrane Proteins. *Nanotechnol. Rev.* **2017**, 6 (1), 15–32. https://doi.org/10.1515/ntrev-2016-0074.

(3) Carpenter, E. P.; Beis, K.; Cameron, A. D.; Iwata, S. Overcoming the Challenges of Membrane Protein Crystallography. *Curr. Opin. Struct. Biol.* **2008**, *18* (5), 581–586. https://doi.org/10.1016/j.sbi.2008.07.001.

(4) Shen, H.-H.; Lithgow, T.; Martin, L. Reconstitution of Membrane Proteins into Model Membranes: Seeking Better Ways to Retain Protein Activities. *Int. J. Mol. Sci.* **2013**, *14* (1), 1589–1607. https://doi.org/10.3390/ijms14011589.

(5) Saotome, K.; Duong-Ly, K. C.; Howard, K. P. Influenza A M2 Protein Conformation Depends on Choice of Model Membrane: Conformation of M2 Protein in Lipid Bilayers. *Biopolymers* **2015**, *104* (4), 405–411. https://doi.org/10.1002/bip.22617.

(6) Kim, S. S.; Upshur, M. A.; Saotome, K.; Sahu, I. D.; McCarrick, R. M.; Feix, J. B.; Lorigan, G. A.; Howard, K. P. Cholesterol-Dependent Conformational Exchange of the C-Terminal Domain of the Influenza A M2 Protein. *Biochemistry* **2015**, *54* (49), 7157–7167. https://doi.org/10.1021/acs.biochem.5b01065.

(7) Mitra, N. Nanodiscs: Membrane Protein Research in Near-Native Conditions. *Mater. Methods* **2013**, 3. https://doi.org/10.13070/mm.en.3.177.

(8) Bayburt, T. H.; Grinkova, Y. V.; Sligar, S. G. Self-Assembly of Discoidal Phospholipid Bilayer Nanoparticles with Membrane Scaffold Proteins. *Nano Lett.* **2002**, 2 (8), 853–856. https://doi.org/10.1021/nl025623k.

(9) Denisov, I. G.; Grinkova, Y. V.; Lazarides, A. A.; Sligar, S. G. Directed Self-Assembly of Monodisperse Phospholipid Bilayer Nanodiscs with Controlled Size. *J. Am. Chem. Soc.* **2004**, *126* (11), 3477–3487. https://doi.org/10.1021/ja0393574.

(10) Hagn, F.; Nasr, M. L.; Wagner, G. Assembly of Phospholipid Nanodiscs of Controlled Size for Structural Studies of Membrane Proteins by NMR. *Nat. Protoc.* **2018**, *13* (1), 79–98. https://doi.org/10.1038/nprot.2017.094.

(11) Bayburt, T. H.; Sligar, S. G. Membrane Protein Assembly into Nanodiscs. *FEBS Lett.* **2010**, *584* (9), 1721–1727. https://doi.org/10.1016/j.febslet.2009.10.024.

(12) Ritchie, T. K.; Grinkova, Y. V.; Bayburt, T. H.; Denisov, I. G.; Zolnerciks, J. K.; Atkins, W. M.; Sligar, S. G. Reconstitution of Membrane Proteins in Phospholipid Bilayer Nanodiscs. In *Methods in Enzymology*; Elsevier, 2009; Vol. 464, pp 211–231. https://doi.org/10.1016/S0076-6879(09)64011-8.

(13) Denisov, I. G.; Sligar, S. G. Nanodiscs for Structural and Functional Studies of Membrane Proteins. *Nat. Struct. Mol. Biol.* **2016**, *23* (6), 481–486. https://doi.org/10.1038/nsmb.3195.

(14) Bayburt, T. H.; Grinkova, Y. V.; Sligar, S. G. Assembly of Single Bacteriorhodopsin Trimers in Bilayer Nanodiscs. *Arch. Biochem. Biophys.* **2006**, *450* (2), 215–222. https://doi.org/10.1016/j.abb.2006.03.013.

(15) Marcink, T. C.; Simoncic, J. A.; An, B.; Knapinska, A. M.; Fulcher, Y. G.;

Akkaladevi, N.; Fields, G. B.; Van Doren, S. R. MT1-MMP Binds Membranes by Opposite Tips of Its β Propeller to Position It for Pericellular Proteolysis. *Structure* **2019**, *27* (2), 281-292.e6. https://doi.org/10.1016/j.str.2018.10.008.

(16) Ito, T.; Gorman, O. T.; Kawaoka, Y.; Bean, W. J.; Webster, R. G. Evolutionary Analysis of the Influenza A Virus M Gene with Comparison of the M1 and M2 Proteins. *J. Virol.* **1991**, *65* (10), 5491–5498.

(17) Liao, S. Y.; Fritzsching, K. J.; Hong, M. Conformational Analysis of the Full-Length M2 Protein of the Influenza A Virus Using Solid-State NMR: Full-Length Influenza M2 Conformation from Solid-State NMR. *Protein Sci.* **2013**, *22* (11), 1623–1638. https://doi.org/10.1002/pro.2368.

(18) Furuse, Y.; Suzuki, A.; Kamigaki, T.; Oshitani, H. Evolution of the M Gene of the Influenza A Virus in Different Host Species: Large-Scale Sequence Analysis. *Virol. J.* **2009**, 6 (1), 67. https://doi.org/10.1186/1743-422X-6-67.

(19) Claridge, J. K.; Mohd-Kipli, F.; Florea, A.; Gate, T.; Schnell, J. R. PH-Dependent Secondary Structure Propensity of the Influenza A Virus M2 Cytoplasmic Tail. *Biomol. NMR Assign.* **2020**, *14* (1), 157–161. https://doi.org/10.1007/s12104-020-09937-8.

(20) Liao, S. Y.; Yang, Y.; Tietze, D.; Hong, M. The Influenza M2 Cytoplasmic Tail Changes the Proton-Exchange Equilibria and the Backbone Conformation of the Transmembrane Histidine Residue to Facilitate Proton Conduction. *J. Am. Chem. Soc.* **2015**, *137* (18), 6067–6077. https://doi.org/10.1021/jacs.5b02510.

(21) Sharma, M.; Yi, M.; Dong, H.; Qin, H.; Peterson, E.; Busath, D. D.; Zhou, H.-X.; Cross, T. A. Insight into the Mechanism of the Influenza A Proton Channel from a Structure in a Lipid Bilayer. *Science* **2010**, *330* (6003), 509–512. https://doi.org/10.1126/science.1191750.

(22) Schnell, J. R.; Chou, J. J. Structure and Mechanism of the M2 Proton Channel of Influenza A Virus. *Nature* **2008**, *451* (7178), 591–595. https://doi.org/10.1038/nature06531.

(23) Stouffer, A. L.; Acharya, R.; Salom, D.; Levine, A. S.; Di Costanzo, L.; Soto, C. S.; Tereshko, V.; Nanda, V.; Stayrook, S.; DeGrado, W. F. Structural Basis for the Function and Inhibition of an Influenza Virus Proton Channel. *Nature* **2008**, *451* (7178), 596–599. https://doi.org/10.1038/nature06528.

(24) Cady, S. D.; Schmidt-Rohr, K.; Wang, J.; Soto, C. S.; DeGrado, W. F.; Hong, M. Structure of the Amantadine Binding Site of Influenza M2 Proton Channels in Lipid Bilayers. *Nature* **2010**, *463* (7281), 689–692. https://doi.org/10.1038/nature08722.

(25) Acharya, R.; Carnevale, V.; Fiorin, G.; Levine, B. G.; Polishchuk, A. L.; Balannik, V.; Samish, I.; Lamb, R. A.; Pinto, L. H.; DeGrado, W. F.; Klein, M. L. Structure and Mechanism of Proton Transport through the Transmembrane Tetrameric M2 Protein Bundle of the Influenza A Virus. *Proc. Natl. Acad. Sci.* **2010**, *107* (34), 15075–15080. https://doi.org/10.1073/pnas.1007071107.

(26) Nguyen, P. A.; Soto, C. S.; Polishchuk, A.; Caputo, G. A.; Tatko, C. D.; Ma, C.; Ohigashi, Y.; Pinto, L. H.; DeGrado, W. F.; Howard, K. P. PH-Induced Conformational Change of the Influenza M2 Protein C-Terminal Domain. *Biochemistry* **2008**, *47* (38), 9934–9936. https://doi.org/10.1021/bi801315m.

(27) Fiorin, G.; Carnevale, V.; DeGrado, W. F. The Flu's Proton Escort. *Science* **2010**,

330 (6003), 456–458. https://doi.org/10.1126/science.1197748.
(28) Thomaston, J. L.; Nguyen, P. A.; Brown, E. C.; Upshur, M. A.; Wang, J.; DeGrado, W. F.; Howard, K. P. Detection of Drug-Induced Conformational Change of a Transmembrane Protein in Lipid Bilayers Using Site-Directed Spin Labeling: Conformational Change of Transmembrane Protein. *Protein Sci.* **2013**, *22* (1), 65–73. https://doi.org/10.1002/pro.2186.
(29) Kim, G.; Raymond, H. E.; Herneisen, A. L.; Wong-Rolle, A.; Howard, K. P. The Distal Cytoplasmic Tail of the Influenza A M2 Protein Dynamically Extends from the Membrane. *Biochim. Biophys. Acta BBA - Biomembr.* **2019**, *1861* (8), 1421–1427. https://doi.org/10.1016/j.bbamem.2019.05.021.
(30) Huang, S.; Green, B.; Thompson, M.; Chen, R.; Thomaston, J.; DeGrado, W. F.; Howard, K. P. C-Terminal Juxtamembrane Region of Full-Length M2 Protein Forms a Membrane Surface Associated Amphipathic Helix: SDSL-EPR of Full-Length M2 Protein. *Protein Sci.* **2015**, *24* (3), 426–429. https://doi.org/10.1002/pro.2631.
(31) Rossman, J. S.; Jing, X.; Leser, G. P.; Lamb, R. A. Influenza Virus M2 Protein Mediates ESCRT-Independent Membrane Scission. *Cell* **2010**, *142* (6), 902–913. https://doi.org/10.1016/j.cell.2010.08.029.
(32) Mchaourab, H. S.; Steed, P. R.; Kazmier, K. Toward the Fourth Dimension of Membrane Protein Structure: Insight into Dynamics from Spin-Labeling EPR Spectroscopy. *Structure* **2011**, *19* (11), 1549–1561. https://doi.org/10.1016/j.str.2011.10.009.
(33) Herneisen, A. L.; Sahu, I. D.; McCarrick, R. M.; Feix, J. B.; Lorigan, G. A.; Howard, K. P. A Budding-Defective M2 Mutant Exhibits Reduced Membrane Interaction, Insensitivity to Cholesterol, and Perturbed Interdomain Coupling. *Biochemistry* **2017**, *56* (44), 5955–5963. https://doi.org/10.1021/acs.biochem.7b00924.
(34) Stepien, P.; Polit, A.; Wisniewska-Becker, A. Comparative EPR Studies on Lipid Bilayer Properties in Nanodiscs and Liposomes. *Biochim. Biophys. Acta BBA - Biomembr.* **2015**, *1848* (1), 60–66. https://doi.org/10.1016/j.bbamem.2014.10.004.
(35) Sahu, I. D.; Lorigan, G. A. Site-Directed Spin Labeling EPR for Studying Membrane Proteins. *BioMed Res. Int.* **2018**, *2018*, 1–13. https://doi.org/10.1155/2018/3248289.
(36) Klug, C. S.; Feix, J. B. Methods and Applications of Site-Directed Spin Labeling EPR Spectroscopy. In *Methods in Cell Biology*; Elsevier, 2008; Vol. 84, pp 617–658. https://doi.org/10.1016/S0091-679X(07)84020-9.
(37) Weil, J. A.; Bolton, J. R.; Wertz, J. E. *Electron Paramagnetic Resonance: Elementary Theory and Practical Applications*; Wiley: New York, 1994.
(38) Berliner, L. J. *Spin Labeling: Theory and Applications.*; Elsevier Science: Saint Louis, 2014.
(39) Weber, R. T. *Xenon User's Guide*; Bruker BioSpin Corporation.
(40) Herneisen, A. L. Conformational Studies of a Domain of the Influenza A M2 Protein Involved in Viral Budding and Morphology, Swarthmore College, 2017.
(41) Wong-Rolle, A. Site-Directed Spin Label EPR Studies of the Interaction Between the Influenza A Proteins (M1 and M2) Involved in Viral Assembly, Swarthmore College, 2019.

(42) Rouck, J. E.; Krapf, J. E.; Roy, J.; Huff, H. C.; Das, A. Recent Advances in Nanodisc Technology for Membrane Protein Studies (2012-2017). *FEBS Lett.* **2017**, *591* (14), 2057–2088. https://doi.org/10.1002/1873-3468.12706.
(43) Kjølbye, L. R.; De Maria, L.; Wassenaar, T. A.; Abdizadeh, H.; Marrink, S. J.; Ferkinghoff-Borg, J.; Schiøtt, B. General Protocol for Constructing Molecular Models of Nanodiscs. *J. Chem. Inf. Model.* **2021**, *61* (6), 2869–2883. https://doi.org/10.1021/acs.jcim.1c00157.
(44) Kozakov, D.; Chuang, G.-Y.; Beglov, D.; Vajda, S. Where Does Amantadine Bind to the Influenza Virus M2 Proton Channel? *Trends Biochem. Sci.* **2010**, *35* (9), 471–475. https://doi.org/10.1016/j.tibs.2010.03.006.
(45) Nayak, D. P.; Hui, E. K.-W.; Barman, S. Assembly and Budding of Influenza Virus. *Virus Res.* **2004**, *106* (2), 147–165. https://doi.org/10.1016/j.virusres.2004.08.012.
(46) Upshur, M. A. SDSL EPR Spectroscopy Reveals Cholesterol Dependent Conformational Shift of Influenza A M2 Protein.
(47) Man, D.; Słota, R.; Kawecka, A.; Engel, G.; Dyrda, G. Liposomes Modified by Mono- and Bis-Phthalocyanines: A Comprehensive EPR Study. *Eur. Phys. J. E* **2017**, *40* (6), 63. https://doi.org/10.1140/epje/i2017-11550-4.